DOKUZ EYLÜL UNIVERSITY

GRADUATE SCHOOL OF NATURAL AND APPLIED SCIENCES

INNOVATIVE CATALYST SYNTHESIS FOR DIRECT ALCOHOL FUEL CELLS

by

Etkin Barış ÇETİN

June, 2019

İZMİR

INNOVATIVE CATALYST SYNTHESIS FOR DIRECT ALCOHOL FUEL CELLS

A Thesis Submitted to the
Graduate School of Natural and Applied Sciences of Dokuz Eylül University
In Partial Fulfillment of the Requirements for the Degree of Master of Science
in Nanoscience and Nanoengineering

by

Etkin Barış ÇETİN

June, 2019
İZMİR

M.Sc THESIS EXAMINATION RESULT FORM

We have read the thesis entitled **"INNOVATIVE CATALYST SYNTHESIS FOR DIRECT ALCOHOL FUEL CELLS"** completed by **ETKİN BARIŞ ÇETİN** under supervision of **ASSOC. PROF. DR. CAN ÖZGÜR ÇOLPAN** and **ASST. PROF. DR. EBRU ERÜNAL** and we certify that in our opinion it is fully adequate, in scope and in quality, as a thesis for the degree of Master of Science.

Assoc. Prof. Dr. Can Özgür ÇOLPAN

Supervisor

Asst. Prof. Dr. Ebru ERÜNAL

Supervisor

Prof. Dr. Hüseyin Günerhan

Jury Member

Prof. Dr. Aytunç EREK

Jury Member

Prof. Dr. Mehmet Kadir Yurdakoç

Jury Member

Prof.Dr. Kadriye ERTEKİN

Director

Graduate School of Natural and Applied Sciences

ACKNOWLEDGEMENTS

Firstly, I would like to represent my deepest gratitude to my supervisors Assoc. Prof. Dr. Can Özgür ÇOLPAN and Asst. Prof. Dr. Ebru ERÜNAL for their endless support, advice, and patience. It was a pleasure to study with them and to have a chance to benefit from their scientific and personal experiences.

I would like to thank Dr. Fatma ULUSAL for her guidance throughout all experiments in the Çukurova University. I would also like to thank Prof. Dr. Mehmet Kadir YURDAKOÇ, Res. Asst. Oylum ÇOLPANAKAN for their academic guidance and help.

Finally, I would like to thank my family for their tolerant attitude to my working effort during enhancement of this thesis and for their sustained support and understanding during all the times of my studies.

Etkin Barış ÇETİN

INNOVATIVE CATALYST SYNTHESIS FOR DIRECT ALCOHOL FUEL CELLS

ABSTRACT

In this thesis work, non-precious nitrogen-doped iron-nickel and iron nanoparticles, supported on three-dimensional reduced graphene oxide, are prepared via a combination of sacrificial support method and wet impregnation method as alternative anode catalysts to precious metal catalysts of the direct methanol fuel cells for electro-oxidation of methanol. Graphene oxide was synthesized via an improved Hummers method. Nitrogen doping was carried out by the pyrolysis of urea, which also provided the reduction of graphene oxide support simultaneously. Electrocatalytic activities of the catalysts for methanol electro-oxidation in acidic media were obtained by cyclic voltammetry (CV). Morphologies of the synthesized materials were obtained using scanning electron microscopy (SEM). The presence and distribution properties of the nanosized iron and nickel particles were detected via scanning electron microscopy-energy dispersive X-ray spectroscopy (SEM-EDS). Quantitative analyses of iron and nickel were conducted by inductively coupled plasma-optical emission spectrometry (ICP-OES). X-ray photoelectron spectroscopy (XPS) analyses were executed to obtain the surface chemical composition and bonding of the synthesized materials and to prove the formation of the alloy. Crystal structures of the materials produced were determined by examining their X-ray diffraction (XRD) patterns. Thermogravimetric analyses (TGA) of the samples were done under a nitrogen atmosphere to obtain their thermal behaviors.

Keywords: Direct methanol fuel cells, methanol electro-oxidation, acidic media, non-precious anode electrocatalysts, nitrogen-doped iron and nickel nanoparticles, three-dimensional reduced graphene oxide support, sacrificial support method, wet impregnation method, graphene oxide, graphene, urea

DOĞRUDAN ALKOLLÜ YAKIT PİLLERİ İÇİN YENİLİKÇİ KATALİZÖR SENTEZİ

ÖZ

Bu tez çalışmasında, üç boyutlu indirgenmiş grafen oksit destekli, değerli olmayan azot katkılı demir-nikel ve demir nanopartikülleri, metanolün elektro-oksidasyonu için doğrudan metanollü yakıt pillerinin değerli metal katalizörlerine alternatif anot katalizörleri olarak kurban destek metodu ve ıslak emdirme metodu kombinasyonu ile hazırlanmıştır. Grafen oksit, geliştirilmiş bir Hummers metodu ile sentezlenmiştir. Azot katkılama, grafen oksit desteğin eş zamanlı olarak indirgenmesini de sağlayan üre pirolizi ile gerçekleştirilmiştir. Katalizörlerin asidik ortamda metanol elektro-oksidasyonu için elektrokatalitik aktiviteleri, dönüşümlü voltametri (CV) ile elde edilmiştir. Sentezlenen malzemelerin morfolojileri, taramalı elektron mikroskobu (SEM) kullanılarak elde edilmiştir. Nano boyutlu demir ve nikel partiküllerinin varlığı ve dağılım özellikleri, taramalı elektron mikroskobu-enerji dağılımlı X-ışını spektroskopisi (SEM-EDS) ile tespit edilmiştir. Demir ve nikelin nicel analizleri, indüktif eşleşmiş plazma-optik emisyon spektrometresi (ICP-OES) ile yapılmıştır. X-ışını fotoelektron spektroskopisi (XPS) analizleri, sentezlenen malzemelerin yüzey kimyasal bileşimini ve bağlarını elde etmek ve alaşım oluşumunu kanıtlamak için gerçekleştirilmiştir. Üretilen malzemelerin kristal yapıları, X-ışını kırınım (XRD) desenlerinin incelenmesi ile belirlenmiştir. Numunelerin termogravimetrik analizleri (TGA), termal davranışlarını elde etmek amacıyla azot atmosferi altında yapılmıştır.

Anahtar kelimeler: Doğrudan metanollü yakıt pilleri, metanol elektro-oksidasyonu, asidik ortam, değerli olmayan anot elektrokatalizörleri, azot katkılı demir ve nikel nanopartikülleri, üç boyutlu indirgenmiş grafen oksit destek, kurban destek metodu, ıslak emdirme metodu, grafen oksit, grafen, üre

CONTENTS

Page

LIST OF FIGURES

Page

CHAPTER ONE
INTRODUCTION

1.1 Introduction

Recent decades, the use of fuel cells as an alternative energy source has increased due to their high efficiency and environmental compatibility (Kim et al., 2014). With the improvements made in the proton exchange membrane (PEM), direct alcohol fuel cells (DAFC) based on proton exchange membrane fuel cells (PEMFC) have become more important especially for transportation applications in virtue of advantages of alcohol which can be used directly as fuel without a bulky and expensive reformer and easily transported and stored (Lamy, Lima, LeRhun, Delime, & Coutanceau, 2002).

However, the comparatively complicated reaction system and the harmful effects of alcohol crossover throughout the membrane are the main problems of the DAFCs. Besides, the methanol (MeOH, 6 kWh/kg), used as fuel in direct methanol fuel cells (DMFC) which is a type of the DAFC, is comparable with gasoline (10-11 kWh/kg) in terms of high energy density. But, carbon monoxide (CO), which is a by-product that blocks the active sites of anode catalysts and occurs during the oxidation of methanol, leads to catalyst poisoning (Lamy et al., 2002).

These problems can be solved by the replacement of platinum, which an expensive catalyst commonly used in fuel cells, with alternative catalysts that can overcome the aforementioned problems. Electrocatalysts that do not include platinum group metal (PGM) which are tried to be developed as an alternative to platinum in recent years, attract the intense interest of the study groups. Non-PGM M (transition metal)-N (nitrogen)-C (carbon) framework catalysts derived from small molecules that exhibit high performance and durability in fuel cell experiments and proposed as a possible candidate to be the substitution of platinum, can be produced by elevated temperature pyrolysis of a metal precursor with a nitrogen/carbon precursor or precursors (Serov, Robson, Artyushkova, & Atanassov, 2012).

Plamen's group has improved the sacrificial support method (SSM) to promote the surface area and active site density of the M-N-C catalysts and to create a three-dimensional (3D) porous structure. The resulting 3D porous structure increased material transport and improved catalytic activity and durability (Atanassov, 2014; Kabir, Serov, Artyushkova, & Atanassov, 2016; Serov, Andersen, et al., 2015; Serov, Robson, Artyushkova, et al., 2012; Serov, Robson, Halevi, Artyushkova, & Atanassov, 2012).

In this method, the catalyst precursors are adsorbed on the template (usually silica) before pyrolysis via wet impregnation or mechanical mixing and the template is removed by etching in potassium hydroxide (KOH) or hydrogen fluoride (HF) after pyrolysis to create the open frame structure of a self-supported material that consists of the catalyst only (Atanassov, 2014).

The Plamen's group produced many different cathode catalysts for oxygen reduction reaction (ORR) with various organic precursors containing different proportions of carbon and nitrogen, such as polyethyleneimine, 4-aminoantipyrine, carbendazim, 4,4'-methylenediantipyrine, 2-aminobenzimidazole, nicarbazin, sulfaguanidine, and mebendazole. In their organic precursor preferences, they considered the criteria high carbon and nitrogen content and low volatility (Robson, Serov, Artyushkova, & Atanassov, 2013; Sebastián et al., 2016; Sebastián et al., 2017; Serov, Artyushkova, Andersen, Stariha, & Atanassov, 2015; Serov, Artyushkova, & Atanassov, 2014; Serov, Robson, Artyushkova, et al., 2012; Serov, Robson, Halevi, et al., 2012; Serov, Robson, Smolnik, & Atanassov, 2012, 2013; Stariha et al., 2016). It is understood, from their bi-metallic and tri-metallic M-N-C ORR catalyst studies with different transition metals that iron is a vital transition metal. In addition, bi-metallic M-N-C catalysts comprised of iron-nickel and iron-manganese exhibited a very strong synergetic effect with high electrocatalytic activity toward ORR and low hydrogen peroxide (H_2O_2) production (Lamy et al., 2002; Serov et al., 2013; Serov, Robson, Smolnik, et al., 2012).

The most important parameters affecting the last ORR activity in acidic media in the production of the Fe-N-C catalysts have determined by the Plamen's group as the temperature of the heat treatment and the rate of iron to precursor containing nitrogen and carbon (Serov et al., 2014; Serov, Robson, Artyushkova, et al., 2012; Serov, Robson, Halevi, et al., 2012) Also, the Plamen's group identified that Fe-Nx centers in Fe-N-C type catalyst were inherently active sites for ORR in acidic media according to observed correlations between surface moieties and ORR performance (Serov et al., 2014).

In different studies, electrocatalysts were dispersed in suitable support to stabilize the catalyst nanoparticles, decrease the quantity of precious metal used, and enhance the durability of the catalyst (Kabir et al., 2016; Lamy et al., 2002; Tylus et al., 2014). The successful distribution of the electrocatalysts was ensured by preferring the carbon-based materials as support owing to their high surface area and electrical conductivity (Lamy et al., 2002). Among the carbon-based materials, graphene stands out as an ideal support candidate with its high surface area, excellent electrical conductivity, and thermal stability. (Alam, Sharma, & Kumar, 2017; Kabir et al., 2016; Tang et al., 2016).

Also, urea (CH_4N_2O) was discovered as the best precursor for nitrogen doping among the different organic substances and inorganic salts as well as has better reducibility (Li et al., 2017).

1.2 Motivation

Having regard to the results and improvements introduced by the Plamen's group to produce open frame self-supported M-N-C type cathode catalysts developed to replace platinum for ORR in acidic media, as well as the remarkable properties of graphene and urea; graphene supported Fe-Ni-N-C anode catalyst containing Fe-Nx centers can be produced to benchmark with platinum in terms of electrocatalytic activity and durability for methanol electro-oxidation in acidic media.

Urea can be preferred as the organic precursor in the production of Fe-Nx species and porous structure, with its carbon and nitrogen content, non-volatility, reducibility and superior success in nitrogen doping.

In addition to its high surface area and excellent electrical conductivity, graphene support can be transformed into a 3D porous structure by the sacrificial support method, and the obtained structure can make significant contributions to catalytic activity and durability by increasing material transport.

1.3 Objectives

The main aim of this thesis is to produce non-precious anode electrocatalysts of the DMFCs as an alternative to precious electrocatalysts, especially platinum, for methanol electro-oxidation in acidic media.

Therefore, non-precious N-doped Fe-Ni and Fe nanoparticles, supported on 3D reduced graphene oxide (N-doped FeNi/rGO, N-doped Fe/rGO), were prepared via a combination of sacrificial support method and wet impregnation method as alternative anode catalysts. Performances of the catalysts also the synergetic effect of the bi-metallic catalyst containing Fe-Ni were investigated by cyclic voltammetry.

A suitable mixing ratio and heat treatment temperature were determined for the precursors and silica used in the catalyst production. The effect of urea used as the organic precursor on the production of Fe-Nx species was determined by X-ray photoelectron spectroscopy. The 3D porous structure desired to be created by the sacrificial support method was examined by scanning electron microscopy. Graphene oxide was prepared, via an improved Hummers (Marcano) method, and reduced to graphene by pyrolysis of urea.

The catalysts produced were analyzed using the physical, chemical and, electrochemical characterization techniques such as SEM, SEM-EDS, XRD, XPS, ICP-OES, TGA, and CV.

1.4 Thesis Outline

This thesis consists of five chapters. In chapter one, general information about state-of-the-art catalysts used in the DAFCs, catalyst materials, the sacrificial support method used in the catalyst production, and also the aim of this thesis are given.

In chapter two, a review of fuel cell technology, particularly on the components and working style of the PEMFCs and DMFCs, is introduced. In addition, catalyst design and graphene are described briefly.

In chapter three, the production of catalysts and graphene oxide is explained step by step. Also, the physical, chemical and electrochemical characterization techniques used in the analyses are mentioned.

In chapter four, the results of the analyses performed using physical, chemical and electrochemical characterization techniques are presented and discussed in detail.

In chapter five, the conclusions of the thesis studies are summarized.

CHAPTER TWO
FUEL CELL TECHNOLOGY

2.1 Fuel Cell

As demonstrated in Figure 2.1, the fuel cell is an energy conversion equipment that can transform the chemical energy of a fuel to electricity by means of a chemical reaction with an oxidizer agent like oxygen, absent any thermal or mechanical process. Today, fuel cells can be used to meet electrical requirements in every aspect of life. Fuel cells work like batteries except with constant flow of oxidizer and fuel. During fuel and oxidizing agent are supplied, they continue to produce electricity and heat without being exhausted (College of the Desert [COD], 2001).

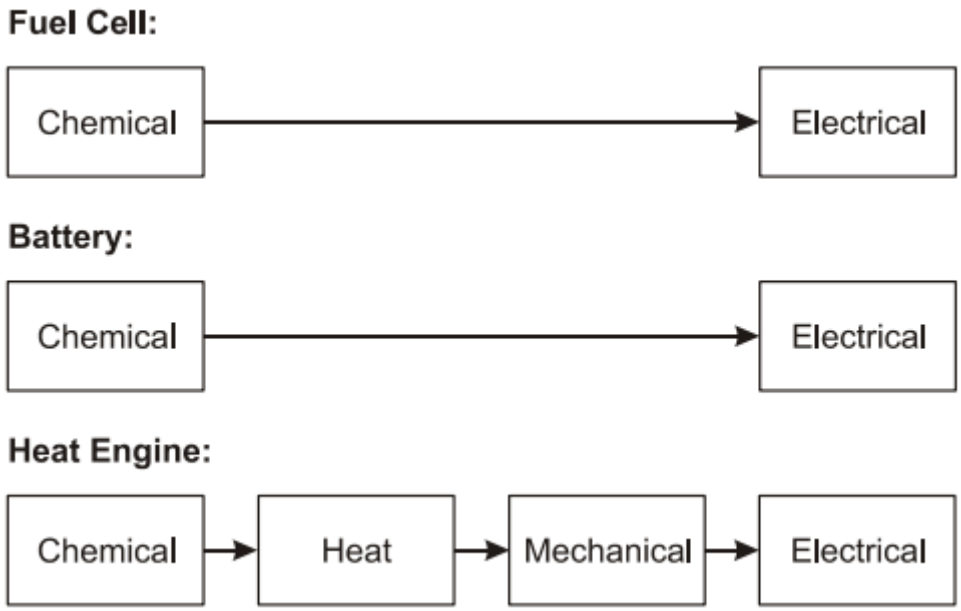

Figure 2.1 Energy transformations for electrical energy output (COD, 2001)

Basically, a fuel cell composes of a negative (anode) electrode and a positive (cathode) electrode connected round the electrolyte. As seen from Figure 2.2, a fuel, like hydrogen, is sent to the anode and an oxidizer, like air, is sent to the cathode. In PEMFCs, catalysts split the hydrogen in order to produce protons and electrons, which go to the cathode using different ways. The electrons pass via an exterior

circuit, constituting electricity flow, while the protons pass throughout the electrolyte to the cathode, where they combine with electrons and the oxygen to form water (COD, 2001).

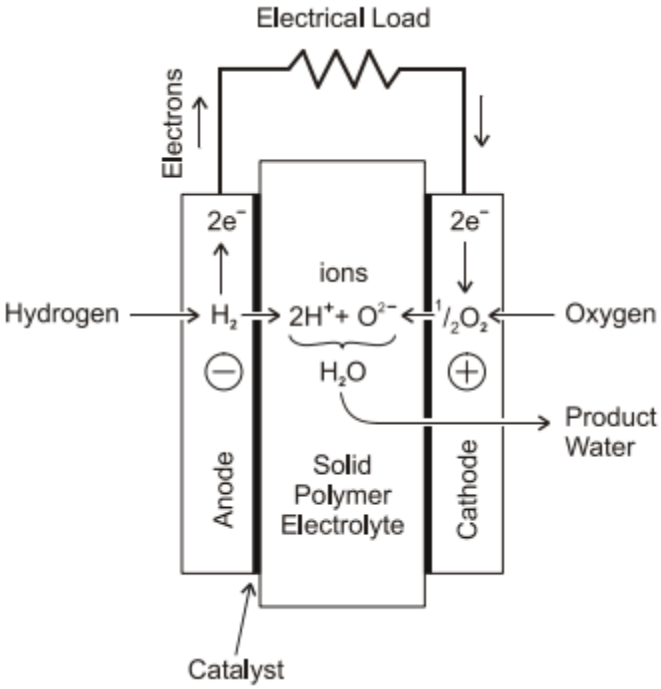

Figure 2.2 The operation system of the PEMFC (COD, 2001)

In the internal combustion engines, the reaction carries out as combustively and heat energy is obtained but in the fuel cells, the reaction carries out electrochemically and electrical energy and heat are obtained (COD, 2001).

2.2 Parts of a Fuel Cell

PEMFCs are consist of many layers of diversified materials as shown in Figure 2.3. The membrane electrode assembly (MEA) also known as the heart of a PEMFC comprises gas diffusion layers (GDLs), catalyst layers, and a membrane. An MEA is incorporated into a fuel cell by hardware components that gaskets which counteract leakage of gases around the MEA, and bipolar plates which supply the fuel and air via own channels and connect individual PEMFCs each other to build a fuel cell stack (COD, 2001).

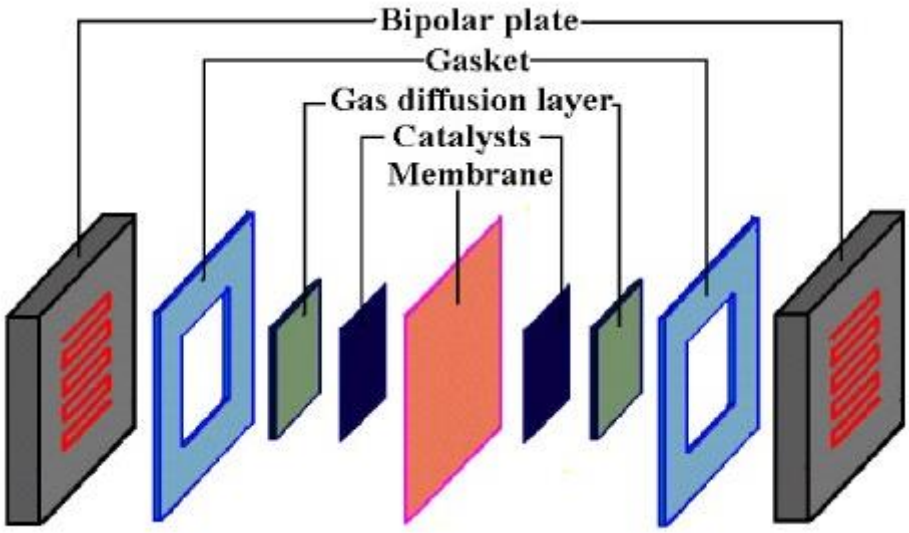

Figure 2.3 Main components of the PEMFC (Technical University of Denmark, 2019)

2.2.1 Membrane Electrode Assembly

The membrane, anode and cathode catalyst layers and GDLs compose the MEA of a PEMFC (COD, 2001).

2.2.1.1 Polymer Electrolyte Membrane

The PEM, also known as the polymer electrolyte membrane, is a solid polymer electrolyte composed of a form of acidified Teflon merely transmitting positive ions throughout the electrolyte and blocks electrons. Other materials going throughout the electrolyte would spoil the chemical reaction and cause a decrease in the performance of the PEMFC (COD, 2001).

2.2.1.2 Catalyst Layers

On both sides of the membrane, there are two catalyst layers, namely the anode catalyst layer which performs the oxidation electrochemical reaction and the cathode catalyst layer which performs the reduction electrochemical reaction. A conventional catalyst layer is obtained by mixing nanoparticles of platinum dispersed on a

convenient carbon support catalysts with an ionomer (ion-conducting polymer) and compressing them among the membrane and the GDLs. While the anode catalyst layer separates the fuel into protons and electrons, the cathode catalyst layer reacts with the protons produced by the anode catalyst layer to accomplish oxygen reduction and provides water formation. The ionomer used in the catalyst layers permits the protons to pass throughout these layers (COD, 2001).

2.2.1.3 Gas Diffusion Layers

The GDLs are found outside the catalyst layer and facilitate passing of the reactants from the catalyst layers, as well as the removing of the formed water. The GDLs are formed of carbon paper layer in which the carbon fibers are in part coated with PTFE (polytetrafluoroethylene). Gases diffuse swiftly across the pores in the GDLs. Excessive water accumulation is prevented by the hydrophobic PTFE which keeps the pores in the GDLs open. The balance between water retention and water discharge must be adjusted to hold membrane conductivity and to keep the pores open so that gases can spread through the electrodes. For this purpose, the surfaces of the GDLs to be added a catalyst layer is covered with a thinnish layer, called the microporous layer which consists of high-surface-area carbon mixed with PTFE (COD, 2001).

2.2.2 Hardware

The MEA which is part of the PEMFC where the energy is generated needs hardware components to work effectively (COD, 2001).

2.2.2.1 Bipolar Plates

A single MEA produces less than 1 volt, so in applications requiring high volts, a plurality of MEAs are combined to form a stack to meet the desired volts as seen in Figure 2.4. Each cell in the stack is separated from an adjacent cell using two bipolar plates which sandwich the MEA. Electrical conduction between the cells in the stack,

as well as physical endurance of the stack, is maintained by these layers which made of metal, carbon, or composites. There are flow fields on the surfaces of the bipolar plate which are set of channels to let gases to flow over the MEA. Also, the bipolar plates may include extra channels to circulate a liquid coolant (COD, 2001).

Figure 2.4 Various PEM fuel cell stacks (COD, 2001)

2.2.2.2 Gaskets

Gaskets made of commonly a rubbery polymer are used to make gas-tight the MEAs compressed between the two bipolar plates (COD, 2001).

2.3 Types of Fuel Cells

Fuel cells are categorized firstly with respect to the type of electrolyte they use. This categorization sets the type of electrochemical reaction to occur in the cell, the type of catalyst required, which fuel to use, and the cell's operating temperature range. These characteristics determine the use of the most suitable fuel cell in the desired application. Special differences between the electrolytes are used to meet the demands of various applications. The fuel and the charged species passing throughout the electrolyte might be different, however the fundamental operations of

all fuel cells are the same. An oxidation reaction takes place at the anode, while a reduction reaction happens at the cathode. These two reactions are brought together by electrons flowing through an exterior circuit and by a charged species passing through an electrolyte (COD, 2001).

2.3.1 Polymer Electrolyte Membrane Fuel Cells

The PEMFCs, also known as the polymer electrolyte membrane fuel cells, produce an elevated power density and have a low weight and bulk in comparison with other fuel cells. As can be seen in Figure 2.5, PEMFCs use a proton-conducting solid polymer membrane as the electrolyte and porous carbon electrodes inclusive a platinum or platinum alloy catalysts. The operating temperatures of the PEMFCs are relatively low at about 80 °C, and they use oxygen and hydrogen to run (COD, 2001). PEMFCs' reactions are shown in Equation (2.1), Equation (2.2), and Equation (2.3).

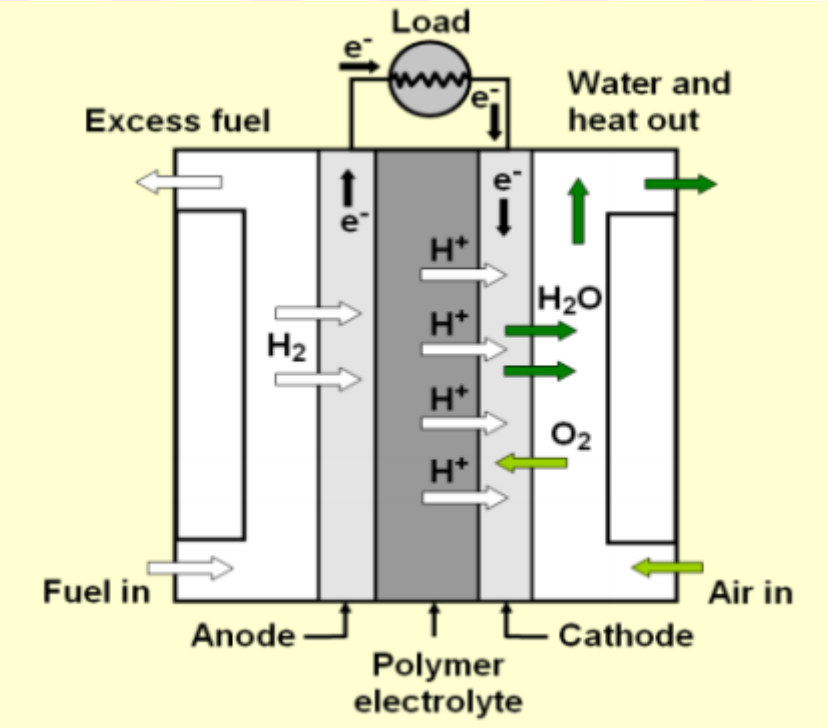

Figure 2.5 Proton exchange membrane fuel cell (Long, Thi, Nogami, & Ohtaki, 2012, chap. 3)

$$\text{Anode: } H_2 \rightarrow 2H^+ + 2e^- \quad (2.1)$$

$$\text{Cathode: } 1/2O_2 + 2H^+ + 2e^- \rightarrow H_2O \quad (2.2)$$

$$\text{Overall reaction: } 1/2O_2 + H_2 \rightarrow H_2O \quad (2.3)$$

However, since PEMFCs run at comparatively low temperatures, they can use hydrocarbon fuels only by converting them to hydrogen in a fuel reformer. Furthermore, the relatively low operating temperature requires the use of expensive noble-metal catalysts such as platinum, and in the case of using hydrogen obtained by converting from hydrocarbon fuels, carbon monoxide poisoning occurs in the platinum catalyst. An additional reactor is needed to reduce the carbon monoxide content of hydrogen obtained by converting from hydrocarbon fuels. Using a fuel reformer and an additional reactor and storing hydrogen are processes that increase the cost. Vice versa, working at low temperatures allows PEM fuel cells to start faster, minimizing wear on system components and maximizing durability. Fast startup time, adequate power-to-weight ratio and the ability to meet rapidly changing power demands make PEMFCs the best candidate for transportation applications. They are also preferred for stationary power applications (COD, 2001).

2.3.2 Direct Methanol Fuel Cells

DMFCs and PEMFCs are similar in that they use a proton-conducting solid polymer membrane as the electrolyte as can be seen in Figure 2.6. DMFCs use methanol directly on the fuel cell's anode without needing a fuel reformer. The methanol used is commonly fed into the system by mixing with water. Methanol has a higher energy density than hydrogen and because it is a liquid it can be stored and transported very easily with today's infrastructure systems. DMFCs are utilized frequently for driving transportable electronic equipments, like cell phones and small batteries (COD, 2001). DMFCs' reactions are shown in Equation (2.4), Equation (2.5), and Equation (2.6).

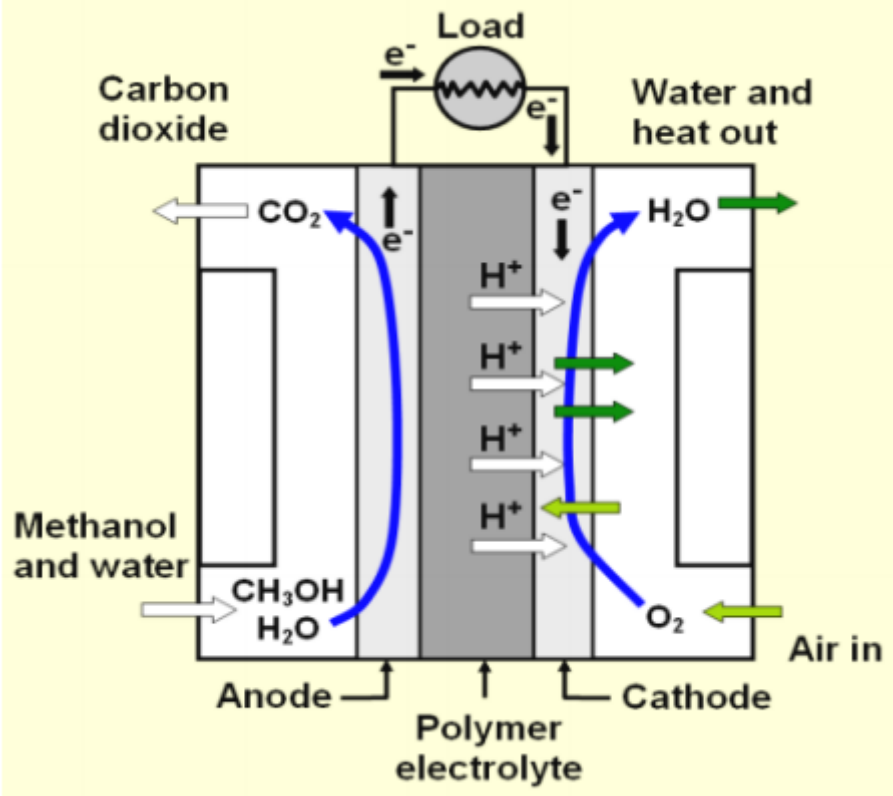

Figure 2.6 Direct methanol fuel cell (Long et al., 2012, chap. 3)

$$\text{Anode: } CH_3OH + H_2O \rightarrow CO_2 + 6H^+ + 6e^- \quad (2.4)$$

$$\text{Cathode: } 3/2O_2 + 6H^+ + 6e^- \rightarrow 3H_2O \quad (2.5)$$

$$\text{Overall reaction: } CH_3OH + 3/2O_2 \rightarrow CO_2 + 2H_2O \quad (2.6)$$

However, DMFCs have some limitations affecting performance. Due to the high concentration of methanol at the anode, the methanol passing from the anode to the cathode throughout the electrolyte carries out, and the oxidation of the passed methanol leads to a combined potential at the cathode and therefore a decrease in the open-circuit voltage. Although there is no need for external humidification in DMFCs, preventing cathode overflows is very important for maintaining performance. DMFCs have slower kinetics due to more complex anode oxidation reactions. In the intermediate reaction steps that make up the methanol oxidation, carbon monoxide, which is considered to be toxic for the platinum catalysts, is generated. Carbon dioxide produced at the anode surface causes a two-phase

countercurrent flow in the anode GDL and may hinder access to the catalyst layer. Methanol is also toxic, highly flammable and miscible in water (COD, 2001).

2.4 Catalyst Design

The structure of the catalyst has a tremendous effect on the electro-oxidation and adsorption of alcohols. The use of a proton exchange membrane, which is an acidic electrolyte, necessitates the selection of stable and active catalysts that can perform the electro-oxidation of alcohols without degradation in this strong acidic environment. Although platinum is preferred at the beginning to meet the desired catalyst properties, catalyst development studies have begun since the platinum is expensive and very sensitive to CO poisoning. Adsorbed CO is a poisoning species that is caused by dissociative chemisorption of alcohol and decreases the productivity of the fuel cell in time by blocking the electroactive sites of the platinum catalyst. Studies have demonstrated that CO poisoning is not effective on highly scattered platinum than on smooth platinum and decreases with increasing roughness. The use of highly dispersed platinum catalysts has resulted in significant reductions in the catalyst loading ratio. However, reducing the platinum loading ratio and weakening the CO poisoning are not permanent solutions (Lamy et al., 2002).

To prevent the generation of adsorbed CO species or to oxidize these species at low potentials, the catalyst structure can be modified by alloying with a second or a third metal so as to alter the adsorption kinetics and oxidation kinetics of the species bounded at the catalyst surface. Ruthenium metal selected for modifying the platinum catalyst has been found to significantly increase the oxidation of alcohols at the platinum surface, especially that of methanol. This synergetic effect is presumed to be a bifunctional mechanism by Watanabe and Motoo in which platinum dissociates methanol with chemisorption and ruthenium creates preferred sites for the adsorption of OH at low potentials by activating water. Adsorbed OH species are essential to oxidize the adsorption residue of alcohol chemisorption to CO_2 entirely (Lamy et al., 2002).

In recent years, non-PGM catalysts with superior properties have been developed to replace the platinum. Non-PGM catalysts can be produced easily by high-temperature pyrolysis of a transition metal precursor with a nitrogen/carbon precursor or precursors (Serov et al., 2012). Besides, the SSM developed by the Plamen's group has enabled these M-N-C type catalysts to have superior catalytic activity and durability in fuel cell experiments by increasing the surface area and active site density and forming a 3D porous structure. The forming 3D porous structure contributes to the development of catalytic activity by increasing material transport (Atanassov, 2013).

2.4.1 Graphene

The catalytic material was dispersed in suitable support in different studies to balance nano catalyst particles, increase the catalyst's durability and decrease the amount of precious metal used. Carbon-based materials having a high surface area and electrical conductivity were chosen as support to provide a high dispersion of the catalytic material (Lamy et al., 2002). Graphene stands out as an ideal support candidate from among the carbon-based materials with its high surface area, perfect electrical conductivity, and thermal stability (Alam et al., 2017; Kabir et al., 2016; Tang et al., 2016).

Graphene is a two-dimensional single atomic layer of graphite composed of sp^2 hybridized carbon atoms. The perfect electronic, mechanical and thermal properties of graphene make it a potential material in many fields such as transistor element, energy storage, gas sensor, and bioelectronic sensor (Alam et al., 2017; Zaaba et al., 2017). Graphene has many properties like high surface area (2620 m^2/g), unique Young's modulus (1 TPa), perfect electron mobility (250000 cm^2/Vs) and thermal conductivity (3000 Wm/K). Graphene can be obtained from graphite using by mechanical exfoliation, epitaxial chemical vapor deposition or chemical means. However, the bulk scale synthesis of graphene can only be provided via chemical means (Alam et al., 2017).

In the chemical methods, graphite is oxidized to graphite oxide using strong oxidizing agents. Graphite oxide is a foliated structure such as graphite, but each layer of carbon atoms in the graphite oxide comprises oxygen-containing functional groups, which broaden the interlayer distance and convert the layers to hydrophilic. Thus these oxidized layers can be readily exfoliated in water via ultrasonication. If the sheets obtained after exfoliation consist of several or less layers of carbon atoms like graphene, they are called graphene oxide. Finally, the obtained graphene oxide can be converted to graphene by removal of the oxygen-containing functional groups (Pei & Cheng, 2012).

The first researcher who found out the unique properties of the graphite oxide was B.C. Brodie. In the Brodie method, graphite and potassium chlorate ($KClO_3$) were mixed in a 1:3 ratio and reacted with fuming nitric acid (HNO_3) for 3 or 4 days at 60 °C. The Brodie method was improved in 1898 by L. Staundenmaier by exchanging two-thirds of fuming HNO_3 to sulfuric acid (H_2SO_4) and using multiple aliquots of $KClO_3$. However, the using of $KClO_3$ caused a continued explosion and took 4 days. Despite these negativities, L. Staundenmaier revealed a new practical method which did not require repetitive oxidation processes. Next, Hummer and Offeman represented their method to prepare graphite oxide in 1958. In this oxidation process, 100g of graphite powder, 50g of sodium nitrate ($NaNO_3$), 2.3-liter H_2SO_4, and 300g potassium permanganate ($KMnO_4$), were used. In Hummer's method, $KMnO_4$ was used to substitute $KClO_3$ to prevent spontaneous explosion while fuming HNO_3 was changed with $NaNO_3$ to annihilate fog acid (Zaaba et al., 2017). Hummer's method emits toxic gases like NO_2 and N_2O_4 and forms the residual Na^+ and NO_3^- ions hard to remove from the wastewater (Chen, Yao, Li, & Shi, 2013; Zaaba et al., 2017). But it can yield high quality graphene oxide within a few hours and prepare more amount of oxygen than the Brodie's method (Zaaba et al., 2017). More recently, Marcano improved Hummer's method by excepting $NaNO_3$, increasing the amount of $KMnO_4$, and using a 9:1 mixture ratio of H_2SO_4/phosphoric acid (H_3PO_4). This method prevents the release of toxic gas and produces a higher amount of hydrophilic carbon material (Chen et al., 2013; Zaaba et al., 2017).

CHAPTER THREE
MATERIALS AND METHODS

3.1 Chemicals

Cab-O-Sil EH-5 fumed silica used as the sacrificial support was provided from Cabot. Other chemicals including graphite powder (particle size < 20 μm) were supplied from Sigma Aldrich. All chemicals were used as obtained.

3.2 Graphene Oxide (GO) Synthesis

GO was synthesized via an improved Hummers (Marcano) method (Marcano et al., 2010; Zaaba et al., 2017). Firstly, 40 ml of 75% H_3PO_4 was added to a 1000 ml beaker and placed to a magnetic stirrer. Subsequently, 360 ml of 96% H_2SO_4 was added to the beaker and mixed for a few minutes (H_2SO_4/ H_3PO_4 ratio 9:1). Then 3 g of graphite powder was added to the acid solution with mixing. 17.6 g of $KMnO_4$ was then little by little supplemented to the solution and the mixture was stirred for 6 hours. Figure 3.1 shows the appearance of the solution after stirring for 6 hours.

Figure 3.1 The appearance of the solution after stirring for 6 hours (Personal archive, 2018)

To annihilate the surplus of $KMnO_4$, the addition of 9 ml of 35% H_2O_2 was performed little by little and mixed for 10 minutes. Afterward, 400 ml of deionized water (DIW) was supplemented to the solution to halt the reaction. Then 135 ml of

30% hydrochloric acid (HCI) was added to the solution under stirring for the removal of the sulfate ion (SO_4^{2-}) and mixed for 20 minutes (Emiru & Ayele, 2017). After mixed, the prepared solution was allowed to stand overnight. Figure 3.2 shows the prepared solution before standing overnight.

Figure 3.2 The prepared solution before standing overnight (Personal archive, 2018)

The supernatant revealed after standing overnight was decanted away, and the remaining precipitate was washed again with DIW and HCI. Figure 3.3 shows the obtained precipitate after standing overnight.

Figure 3.3 The obtained precipitate after standing overnight (Personal archive, 2018)

The resulting solution was transferred to Gooch crucibles for vacuum filtration. Figure 3.4 shows the vacuum filtration setup used.

In the Gooch crucibles, while washing with HCI and DIW continues, it can be checked that the SO_4^{2-} is completely removed by adding barium chloride ($BaCl_2$) to the liquids collected in Büchner flasks. If SO_4^{2-} is present in the collected liquids, a white precipitate will form when $BaCl_2$ added; if not, the washing is continued only with DIW (Emiru & Ayele, 2017).

DIW was added to the solutions in the Gooch crucibles by mixing with the glass rod until collected liquids in the Büchner flasks reached the neutral pH.

Figure 3.4 The vacuum filtration setup used (Personal archive, 2018)

After completion of the vacuum filtration, the remaining solid GO in the Gooch crucibles was dried at 85 °C overnight in a furnace without being removed from the Gooch crucibles. Figure 3.5 shows the remaining solid GO in the Gooch crucible after completion of the vacuum filtration.

Figure 3.5 The remaining solid GO in the Gooch crucible after completion of the vacuum filtration (Personal archive, 2018)

About 5.6 g dried GO was obtained from the Gooch crucibles and pulverized to a fine powder using a mortar and pestle.

3.3 Catalyst Preparation

5 g of the synthesized GO was wholly exfoliated, in 500 mL of DIW using an ultrasonic bath for 1.5 hours. Meanwhile, 5 g of the EH-5 fumed silica (Cab-O-Sil, surface area 380 m^2/g) was dispersed in DIW using an ultrasonic bath (Silica/GO weight ratio 1:1). Later on, the silica and the GO solutions were mixed and ultrasonicated for 25 minutes. After ultrasonication, the solution was divided into two separate beakers. Then 1.25 g of iron nitrate ($Fe(NO_3)_3.9H_2O$) and 2.5 g of urea were added into the beaker; meantime 0.9375 g of iron nitrate, 0.3125 g of nickel nitrate ($Ni(NO_3)_2.4H_2O$) and 2.5 g of urea were added into the other beaker. The beakers were ultrasonicated for 3.5 hours. The metal precursors ratio (iron nitrate/nickel nitrate) was selected as 3:1 by mass. After ultrasonication, solutions of silica-iron nitrate-nickel nitrate-GO-urea and silica-iron nitrate-GO-urea were poured into two separate rectangular flat pyrex glass containers and dried at 85°C overnight. Figure 3.6 shows one of the solids obtained after dried overnight.

Figure 3.6 One of the solids obtained after dried overnight in a rectangular flat pyrex glass container (Personal archive, 2018)

The obtained solids were pulverized to fine powders using a mortar and pestle. The powders were then exposed to heat treatment at 850°C for 1 hour under ultrahigh pure (UHP) nitrogen gas atmosphere with a flow rate of 0.8 NI/min (101.3 kPa air at 20°C) and a temperature ramp rate of 10 °C/min to decompose the organic precursor urea, reduce the GO and provide simultaneous nitrogen doping. After completed heat treatment, the leaching of the silica was conducted by 25 wt% HF overnight (10 ml of HF per 1 g of silica). Last, the resulting powders were washed with DIW until the neutral pH was reached and dried at 85°C overnight. The dried powders were pulverized to fine powders using a mortar and pestle before the second heat treatment. The second heat treatment was carried out under the same conditions.

3.4 Physical and Chemical Characterization

Morphologies of the synthesized materials were obtained using scanning electron microscopy (SEM, COXEM EM-30 Plus). The presence and distribution properties of the nanosized iron and nickel particles were detected via scanning electron microscopy-energy dispersive X-ray spectroscopy (SEM-EDS, JOEL JSM-6060). Crystal structures of the materials produced were determined by examining their X-ray diffraction (XRD) patterns (Rigaku Miniflex, CuK_{α} λ= 0.154 nm radiation). X-ray photoelectron spectroscopy (XPS) analyses were executed on a Thermo Scientific K-Alpha to obtain the surface chemical composition and bonding of the

synthesized materials and to prove the formation of the alloy. Quantitative analyses of iron and nickel were conducted by inductively coupled plasma-optical emission spectrometry (ICP-OES, Perkin Elmer 2100 DV). Thermogravimetric analyses (TGA) of the samples were done under a nitrogen atmosphere with a heating rate of 10 °C/min to obtain their thermal behaviors (Perkin Elmer STA 6000).

3.5 Electrochemical Characterization

Cyclic voltammetry (CV) measurements were done in 0.5 M H_2SO_4 electrolyte that contains 1.0 M MeOH at a scan rate of 100 mV/s between -1.0 V - 2.0 V to determine the electrocatalytic activities of the synthesized catalysts towards methanol electro-oxidation (GAMRY INSTRUMENTS Interface 1000 Potentiostat/Galvanostat/Zero Resistance Ammeter). A three-electrode configuration was used in the electrochemical tests. Ag/AgCl and Pt were used as a reference and counter electrodes respectively. 12.6 mg of N-doped Fe/rGO and 11.6 mg of N-doped FeNi/rGO catalysts were used to prepare the working electrodes with a surface area of 1 cm^2. The synthesized catalysts were mixed with polyvinylidene fluoride (PVDF) (10% by mass) and 0.05 ml dimethylformamide (C_3H_7NO). The mixtures were applied on the graphite electrodes' surface. The prepared electrodes were kept in a furnace at 80°C overnight before measurements.

CHAPTER FOUR
RESULTS AND DISCUSSION

4.1 SEM Analyses

The porous structure of the synthesized catalysts was observed unambiguously from Figure 4.1 and Figure 4.2. This improved porous structure forms by the removal of the silica template and decomposition of the organic network of urea (Stariha et al., 2016).

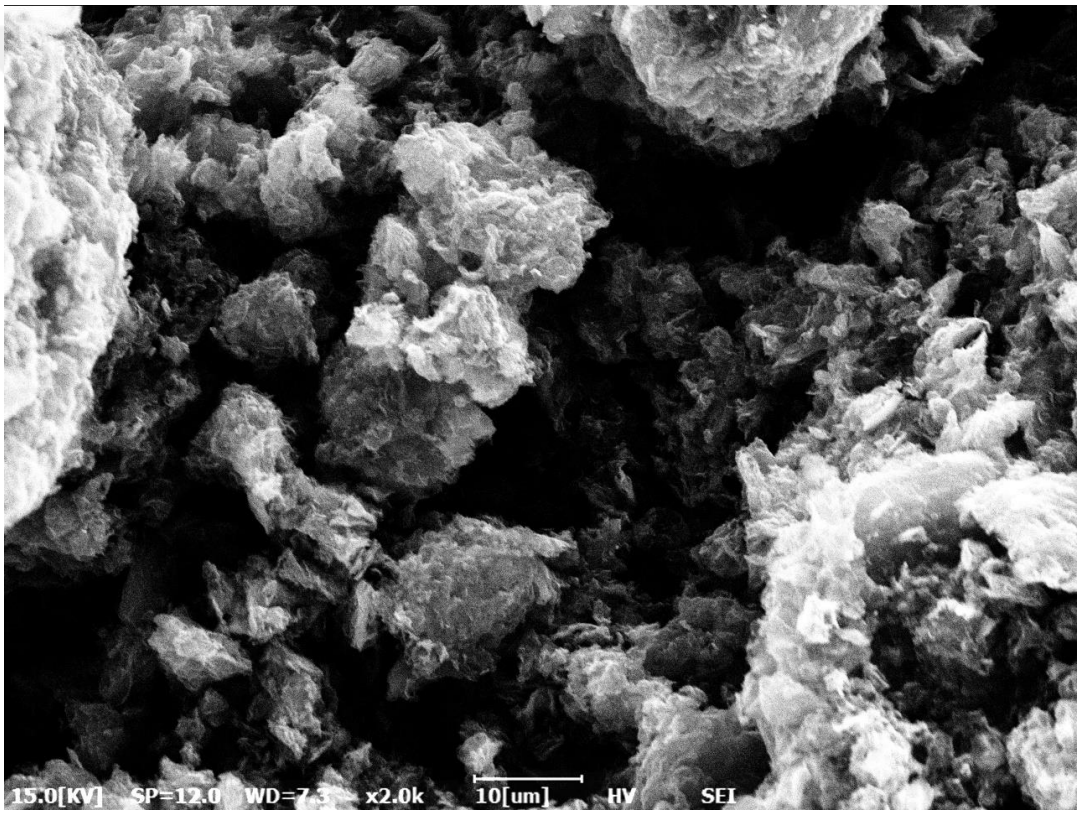

Figure 4.1 SEM image of N-doped Fe/rGO

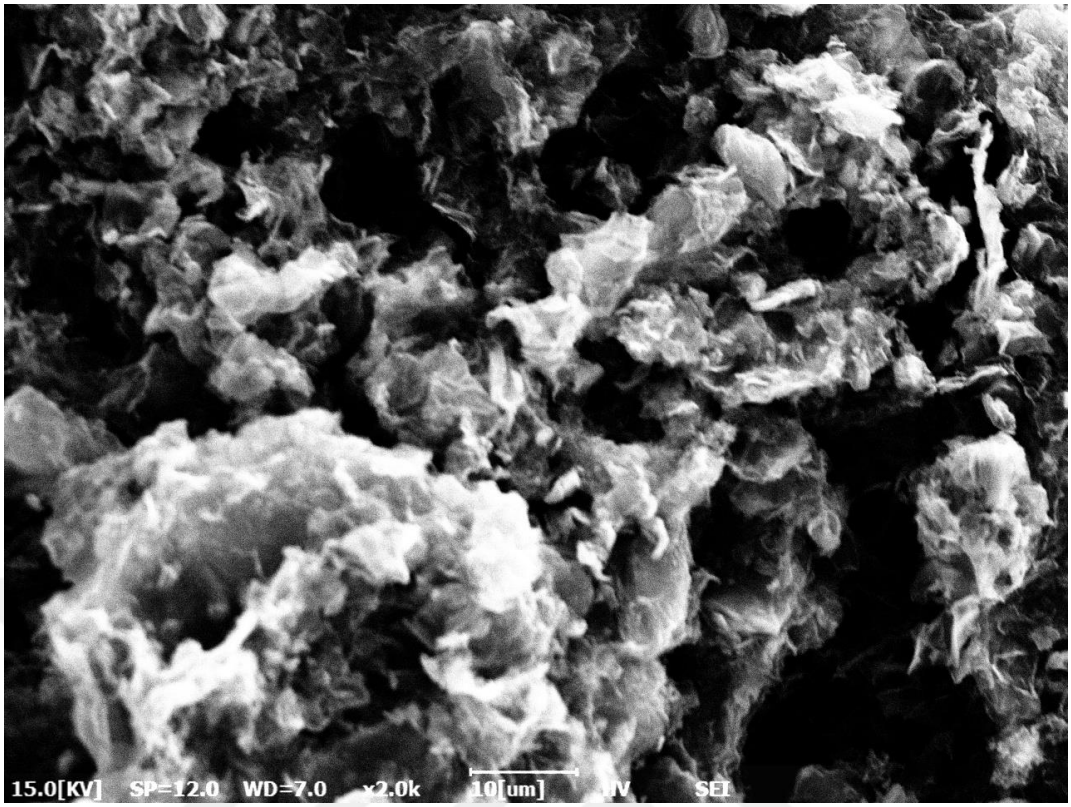

Figure 4.2 SEM image of N-doped FeNi/rGO

From the SEM images, it is obvious that catalysts have the 3D porous structure which provides to circumvent the stacking of the graphene sheets (Tang et al., 2016). Although the catalysts contain different components, there is almost no difference in the resulting images. Because the resulting porous structure is directly caused by the sacrificial support method, thereby increasing the surface area and improving the catalytic performance (Serov et al., 2013; Serov, Robson, Smolnik, et al., 2012).

4.2 SEM-EDS Analyses

The presence of the nanosized iron and nickel particles and their homogeneous distribution over the graphene layer were detected in Figure 4.3 and Figure 4.4. The exact overlap of the figures showing the distribution of iron and nickel metals in some regions indicates the presence of the Fe-Ni alloy in part (El-Deen, El-Newehy, Kim, & Barakat, 2015).

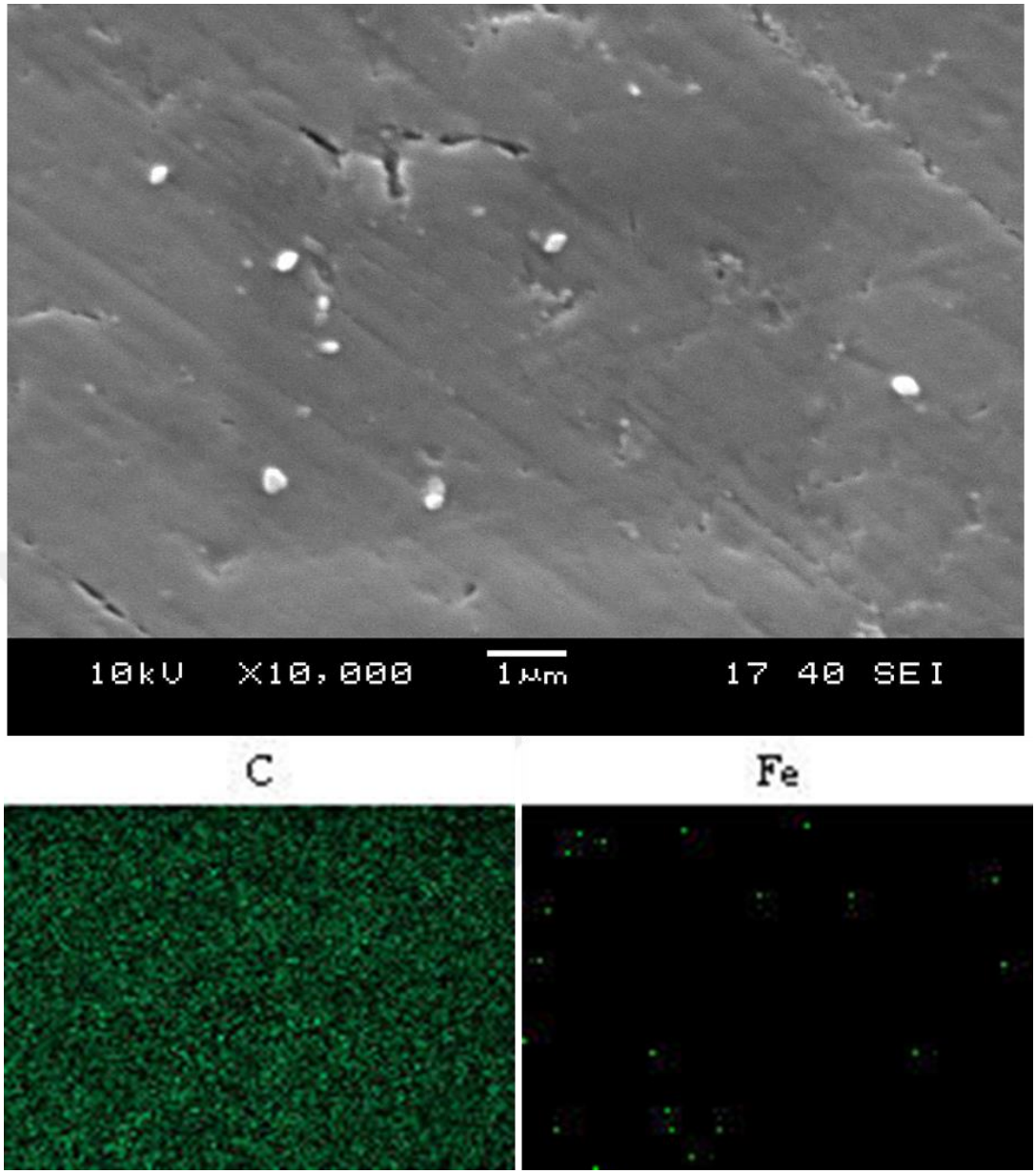

Figure 4.3 SEM-EDS image of N-doped Fe/rGO

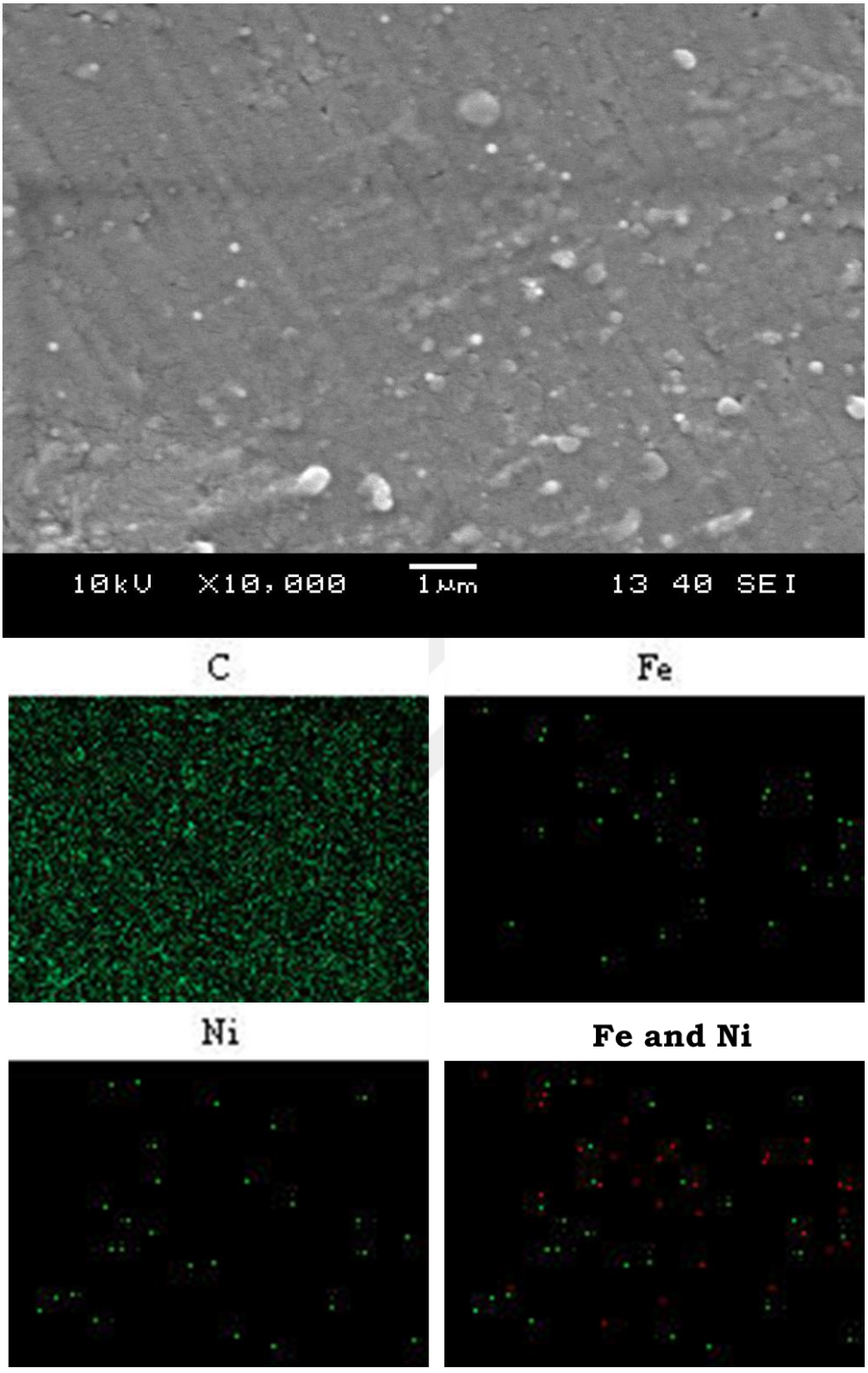

Figure 4.4 SEM-EDS image of N-doped FeNi/rGO

4.3 XRD Analyses

Figure 4.5 demonstrates XRD patterns of the GO (without extra exfoliation process), N-doped Fe/rGO catalyst and N-doped FeNi/rGO catalyst. The graphite has a sharp peak at ~26°, and the graphene interlayer distance within is 0.34 nm. When the graphite is oxidized to form graphite oxide, the peak at ~26° vanishes and a new peak formation at ~11° is observed. Commonly, the GO interlayer distance in the graphite oxide is about 0.6-1.0 nm dependently on the oxidation level of the graphite and the number of intercalated water molecules (Jianchang Li, Zeng, Ren, & van der Heide, 2014).

The prepared GO has two distinct peaks at 11.16° and 42.73°. The peak at 11.16° corresponds to the (001) diffraction plane with an interlayer distance of 7.92 Å. The interlayer distance of 7.92 Å is owing to the existence of oxygen-containing functional groups in the GO which are introduced by the oxidation of the graphite (Alam et al., 2017; Jianchang Li et al., 2014; Pendolino & Armata, 2017, chap. 2). The absence of a peak at ~26° and the interlayer distance of 7.92 Å without extra exfoliation process show the efficiency of the Marcano method to obtain GO.

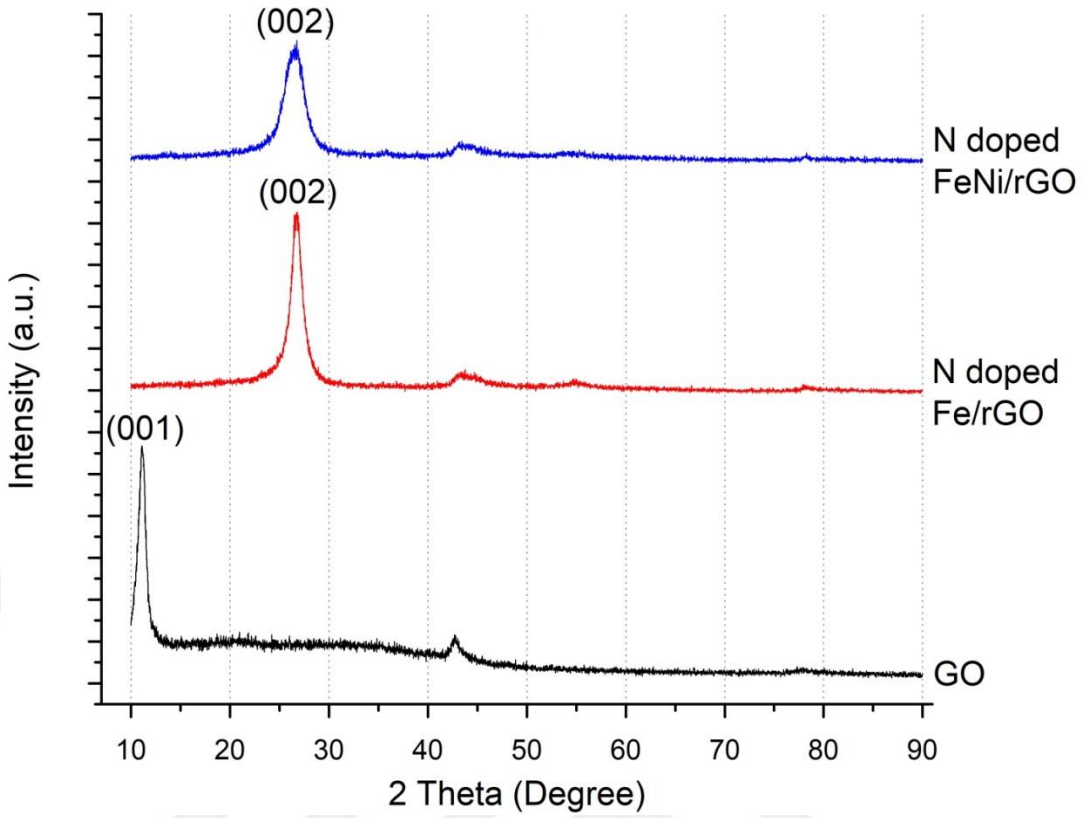

Figure 4.5 XRD results of GO, N-doped Fe/rGO and N-doped FeNi/rGO

After thermal reduction, the disappearance of the peak at 11.16° and the formation of the new peak at ~26° on the XRD patterns of the catalysts indicates that GO nanosheets are reduced to graphene nanosheets successfully. The peak at ~26° on the XRD patterns of the catalysts corresponds to the (002) diffraction plane with interlayer distances of 3.36 Å and 3.34 Å for N-doped FeNi/rGO and N-doped Fe/rGO respectively. (Alam et al., 2017; Liu, Zhao, Gao, Jiang, & Zeng, 2013). The decrease in the interlayer distances stems from the subtraction of oxygen-containing functional groups and intercalated water molecules (Barakat, El-Deen, Ghouri, & Al-Meer, 2018).

The peaks at 43.44°, 50.34°, and 74.24° on the XRD pattern of N-doped FeNi/rGO corresponding to the (111), (200), (220) diffraction planes respectively, confirm the formation of the Fe-Ni alloy barely because of low intensities of the peaks (Barakat et al., 2018; Juan Li et al., 2018). The XRD patterns of the catalysts are very similar in spite of containing different components. The average crystallite

size of the N-doped FeNi/rGO and N-doped Fe/rGO catalysts was calculated via the Scherrer equation as 2.8 nm and 4 nm respectively. The Scherrer equation is given in Equation (4.1) where L is the average crystallite size, K is the Scherrer constant (0.89) associated with crystallite shape, λ is the X-ray wavelength (0.154056 nm), β is the full width at half maximum of the diffraction peak in radians and θ is Bragg's diffraction angle (A. Monshi, Foroughi, & M. R. Monshi, 2012; Kabir et al., 2016).

$$L = \frac{K\lambda}{\beta\cos\theta} \tag{4.1}$$

4.4 XPS Analyses

As shown in Figure 4.6, the C 1s XPS spectrum of GO demonstrates a remarkable oxidation level that corresponds to different carbon-containing functional groups, these are the non-oxygenated ring C (~284.6 eV), the C in C-O bonds (~286.0 eV), the carbonyl C (~287.8 eV), and the carboxylate carbon (O-C=O, ~289.0 eV) (Pei & Cheng, 2012).

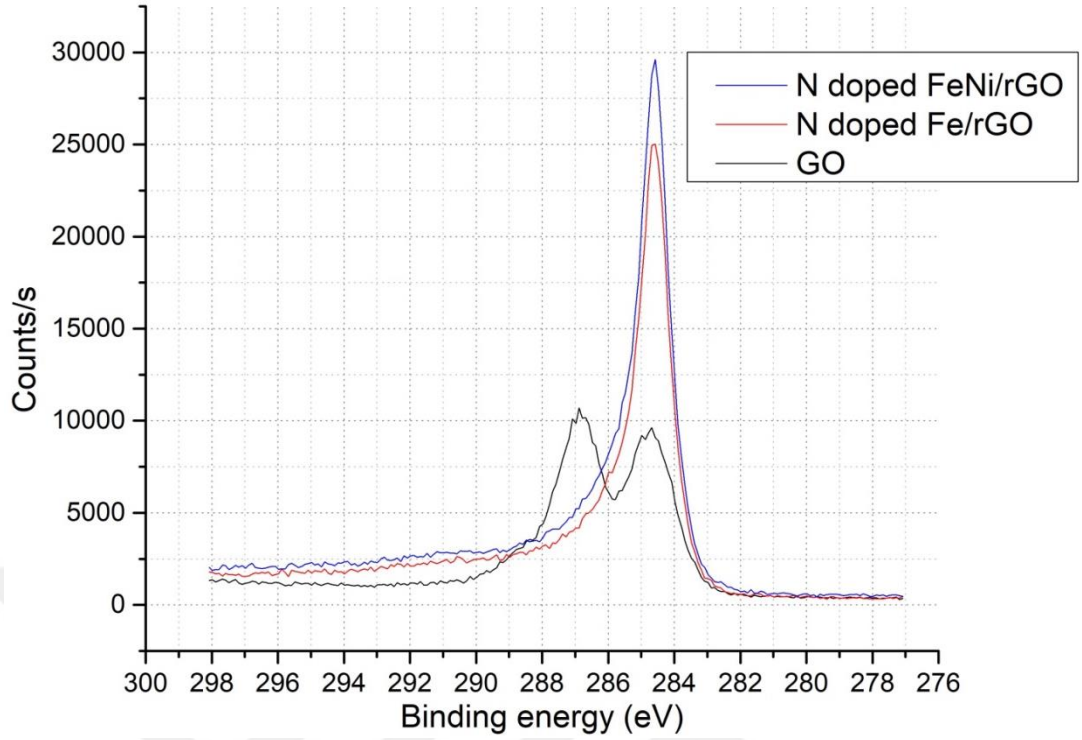

Figure 4.6 The C 1s XPS spectra of GO, N-doped Fe/rGO and N-doped FeNi/rGO

The high level of oxidation and the resulting oxygen-containing functional groups reaffirm the efficiency of the Marcano method in the production of graphene oxides. According to the C 1s XPS spectra of N-doped Fe/rGO and N-doped FeNi/rGO, the main peak remaining after thermal reduction was the non-oxygenated ring C at ~284.6 eV corresponding to the graphite-like sp^2 C and the oxygen-containing functional groups were removed successfully (Wei et al., 2009; X. Li et al., 2009). Also, in the C 1s XPS spectra of the catalysts, a small increase was observed at 285.8 eV corresponding to the N-sp^2 C bond (Wei et al., 2009). A higher degree of sp^2 carbon hybridization of the thermally reduced catalysts was considered significant to increase the activity of the electrocatalysts for ethanol electro-oxidation (Kabir et al., 2016). Furthermore, as a new observation, the Plamen's group has correlated the amount of surface carbon oxides with the ORR in acidic media (Serov, Artyushkova, et al., 2015).

Figure 4.7 shows N 1s XPS spectra of the N-doped Fe/rGO and N-doped FeNi/rGO catalysts. According to the N 1s XPS spectra, N doping was confirmed as

8.27% and 6.36% for N-doped FeNi/rGO and N-doped Fe/rGO respectively. The N 1s spectrum corresponds to species such as imide or cyano-N (398.0 eV), pyridinic nitrogen (398.6 eV), nitrogen coordinated to iron (Fe-Nx, 399.6 eV), pyrrolic nitrogen (400.7 eV), quaternary nitrogen (401.5 eV), graphitic nitrogen (403 eV), and N-O (405-407 eV) typically found in the M-N-C catalysts (Serov, Artyushkova, et al., 2015).

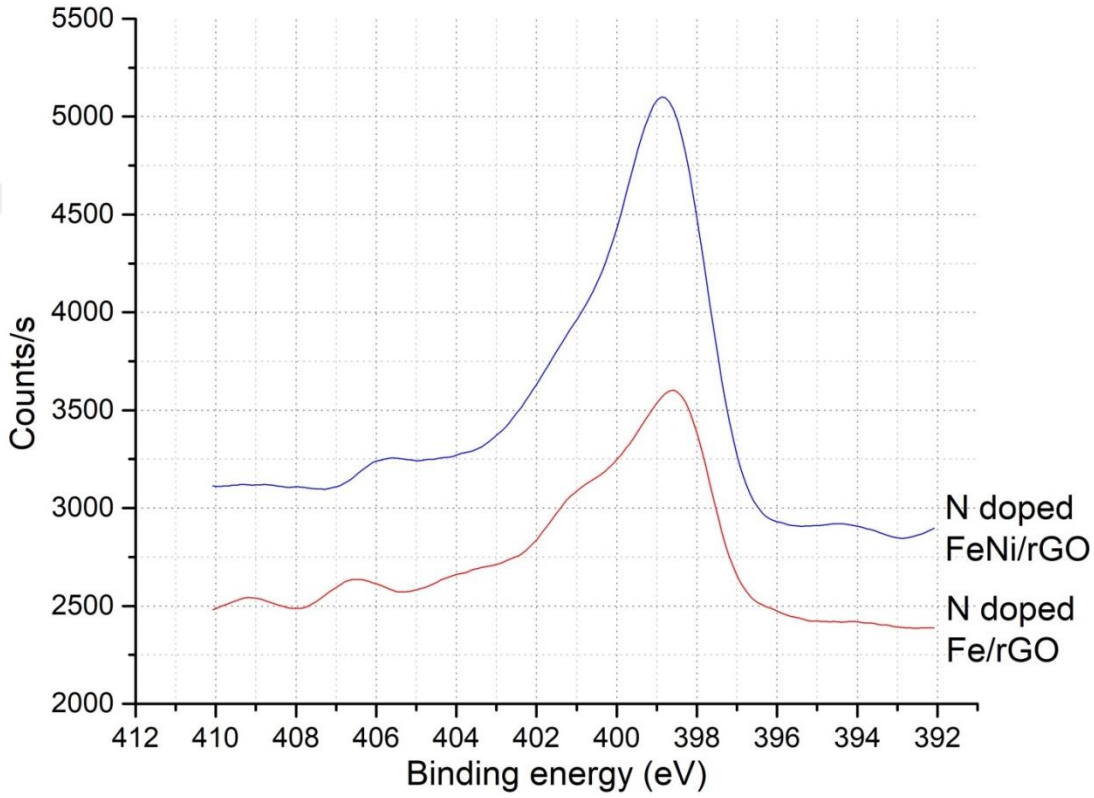

Figure 4.7 The N 1s XPS spectra of N-doped Fe/rGO and N-doped FeNi/rGO

The prepared catalysts consisted of mainly pyridinic nitrogen (398.6 eV) and Fe-Nx (399.6 eV) which were the moieties that suggested to be most directly related to the increase in ORR activity in acidic media (Sebastián et al., 2016; Serov et al., 2014; Serov, Artyushkova, et al., 2015; Serov, Robson, Artyushkova, et al., 2012; Stariha et al., 2016). However, studies with Fe-N-C type catalysts have shown that ORR activity in acidic media was dramatically reduced in the absence of iron, even if the amount of pyridinic nitrogen was very high (Serov et al., 2014). In addition, when the iron was removed from high-performance bi-metallic and tri-metallic M-N-

C catalysts consisting of iron and different transition metal or metals (cobalt, copper, nickel, manganese), significant decreases in ORR activity in acidic media were observed again (Serov et al., 2013; Serov, Robson, Smolnik, et al., 2012). According to these results, for high ORR activity in acidic media, the Fe-Nx centers are the most important active sites, and iron is essential. The fact that the prepared catalysts contain high amounts of the pyridinic nitrogen and Fe-Nx centers indicates that they may have elevated catalytic activity also towards the ORR in acidic media.

The pyridinic nitrogen and Fe-Nx centers were also identified as the fundamental centers accountable for H_2O_2 reduction to water in acidic media (Serov, Artyushkova, et al., 2015), Pyrrolic nitrogen, quaternary nitrogen, and graphitic nitrogen were specified, as the main centers responsible for H_2O_2 generation (Serov, Artyushkova, et al., 2015; Serov, Robson, Artyushkova, et al., 2012). The fact that the prepared catalysts contain low amounts of pyrrolic nitrogen, quaternary nitrogen, and graphitic nitrogen centers indicates that they may have low H_2O_2 production and thus high durability. Since H_2O_2 is a chemically active by-product, it causes the corrosive effect on the carbonaceous catalyst support, membrane and ionomer (Serov, Robson, Smolnik, et al., 2012).

As shown in Figure 4.8, Ni 2p XPS spectrum for N-doped FeNi/rGO at 851.7 eV equals to metallic Ni and the peaks at 854.8 eV and 872 eV belong to Ni^{2+} of Ni-O bond and Ni^{2+} respectively. The doping amount of Ni was 3.28% for N-doped FeNi/rGO according to Ni 2p XPS spectrum (Jing et al., 2016; Yang, Zeng, Wang, & Cao, 2018).

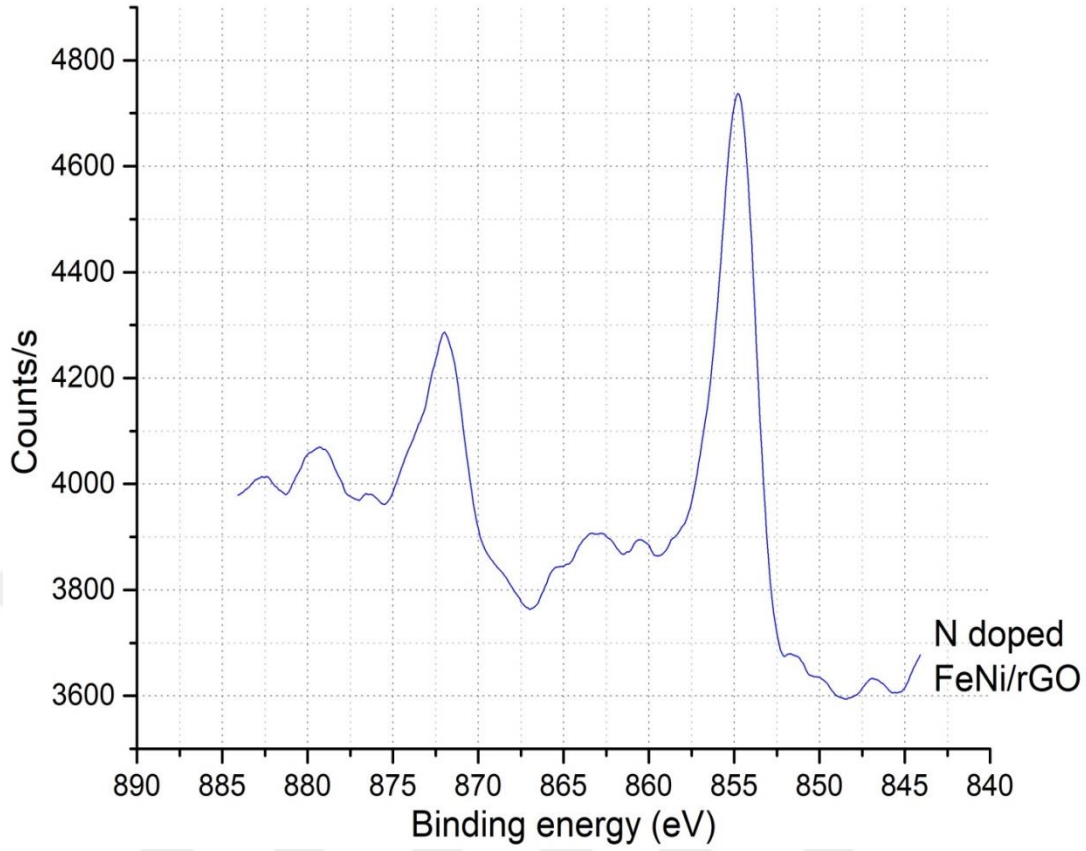

Figure 4.8 The Ni 2p XPS spectrum of N-doped FeNi/rGO

Figure 4.9 shows Fe 2p XPS spectra of the N-doped Fe/rGO and N-doped FeNi/rGO catalysts. The Fe 2p XPS spectrum for N-doped Fe/rGO at 705.2 eV indicates the presence of metallic Fe. The Fe 2p XPS spectrum for N-doped FeNi/rGO at 706.8 eV and 721.2 eV correspond to metallic Fe in the Fe-Ni alloy. Furthermore, the peaks presented at ~711.4 eV and ~724.4 eV in the Fe 2p XPS spectra can be attributed to the Fe-Nx species (Jing et al., 2016; Yang et al., 2018). The doping amounts of Fe were 4.10% and 3.49% for N-doped Fe/rGO and N-doped FeNi/rGO respectively according to Fe 2p XPS spectra.

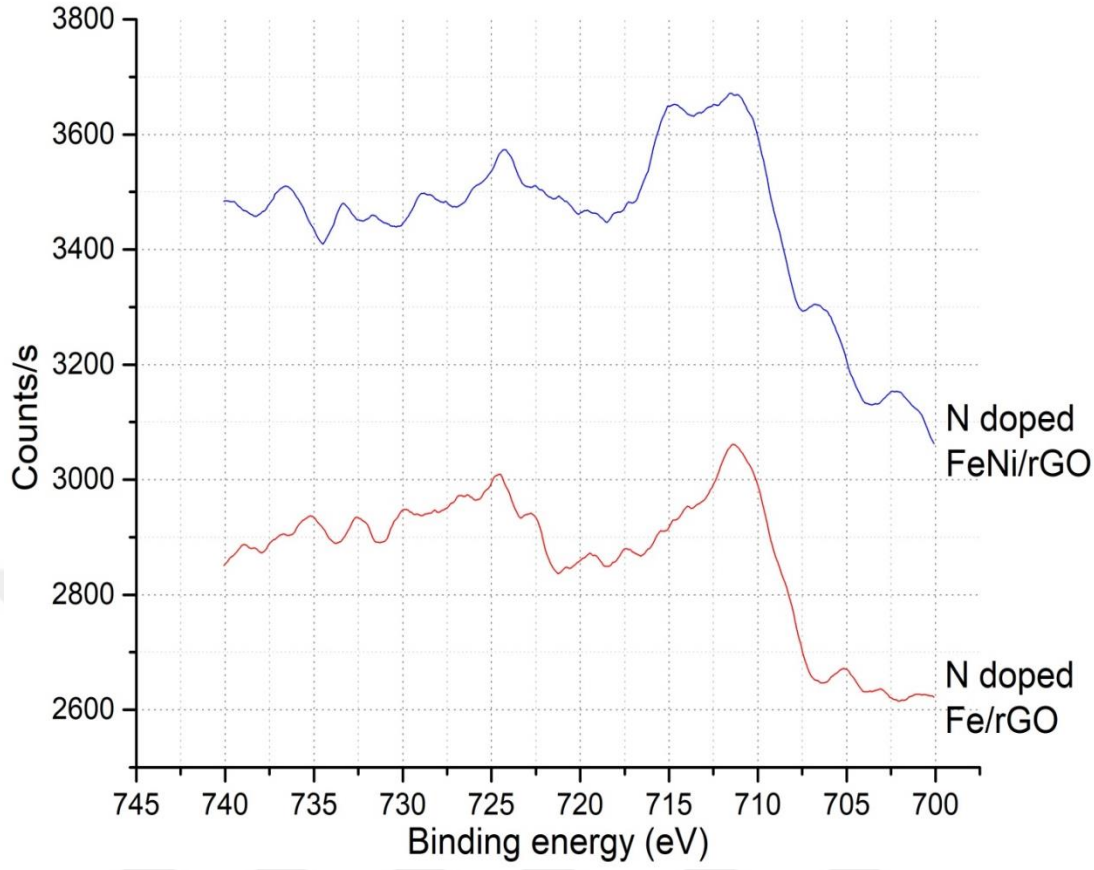

Figure 4.9 The Fe 2p XPS spectra of N-doped Fe/rGO and N-doped FeNi/rGO

4.5 ICP-OES Analyses

According to the ICP-OES results, the N-doped FeNi/rGO catalyst contained 6.27 wt% Fe and 3.04 wt% Ni, while N-doped Fe/rGO catalyst contained 7.215 wt% Fe.

4.6 TGA Analyses

The thermal behaviors of the GO, N-doped Fe/rGO and N-doped FeNi/rGO were acquired by TGA in a nitrogen atmosphere and shown in Figure 4.10. The weight loss is 8.5% between 30°C and 100 °C and ascribed to the evaporation of physisorbed water in the GO (Alam et al., 2017; Cote, Cruz-Silva, & Huang, 2009; Dimiev, Alemany, & Tour, 2013; Xu, Li, & Huang, 2017).

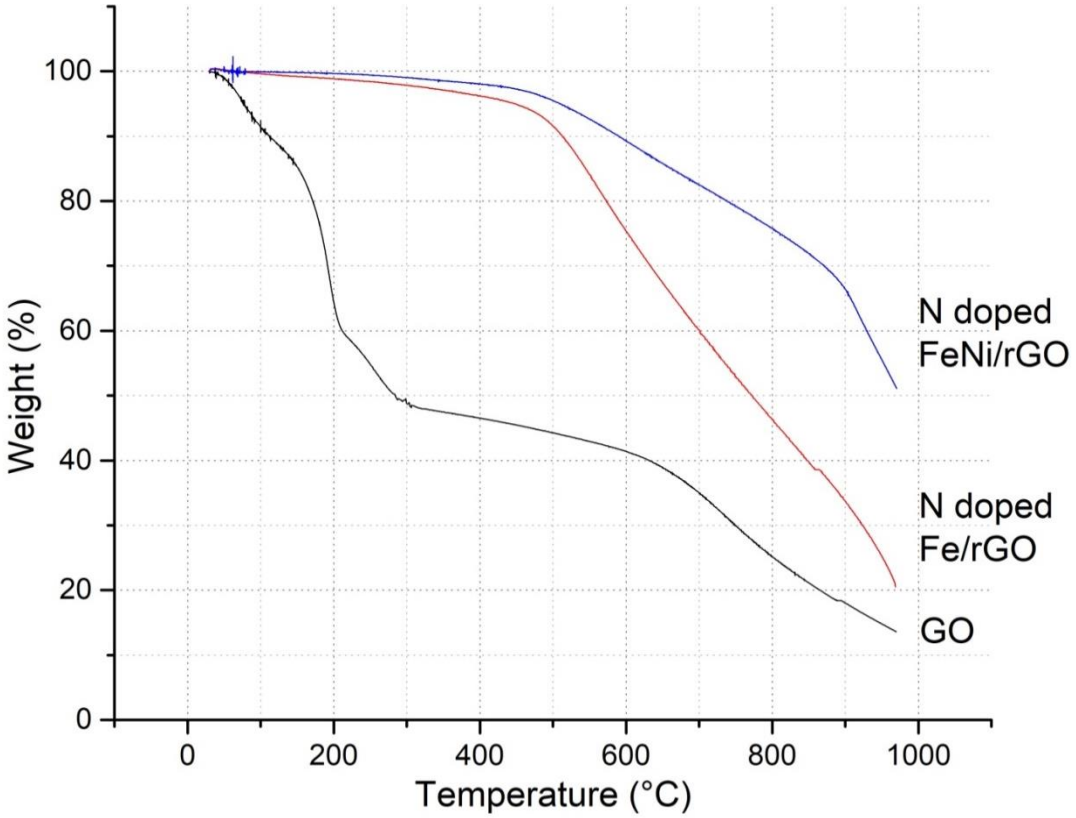

Figure 4.10 TGA curves of GO, N-doped Fe/rGO and N-doped FeNi/rGO

The weight loss between 100 °C and 160 °C is 8.3 % and caused by the evaporation of chemisorbed water in the GO (Xu et al., 2017). The weight loss between 160°C and ~ 600°C is 41.8 % owing to the subtraction of the oxygen-containing functional groups in the GO (Alam et al., 2017; Cote et al., 2009; Dimiev et al., 2013; Juan Li et al., 2018; Liu et al., 2013; X. Li et al., 2009; Xu et al., 2017). The weight loss between ~ 600°C and 970°C is 27.8% and attributed to oxidation of carbon and subtraction of the oxygen-containing functional groups in the GO (Alam et al., 2017; Juan Li et al., 2018; Liu et al., 2013; X. Li et al., 2009; Xu et al., 2017). The weight losses between 30°C and 460°C are 3% and 4.5% for N-doped FeNi/rGO and N-doped Fe/rGO respectively and stem from removal of the oxygen-containing functional groups (Alam et al., 2017; Cote et al., 2009; Dimiev et al., 2013; Juan Li et al., 2018; Liu et al., 2013; X. Li et al., 2009; Xu et al., 2017). These low weight losses prove the subtraction of the oxygen-containing functional groups in the GO. The weight losses between 460°C and 970°C are 45.8% and 74% for N-doped FeNi/rGO and N-doped Fe/rGO respectively arose from the oxidation of rGO and

removal of the oxygen-containing functional groups (Alam et al., 2017; Juan Li et al., 2018; Liu et al., 2013; X. Li et al., 2009; Xu et al., 2017). N-doped FeNi/rGO has higher thermal stability and lower weight loss than that of N-doped Fe/rGO due to containing higher metal content.

4.7 CV Analyses

Cyclic voltammetry measurements were created in 0.5 M H_2SO_4 electrolyte that contains 1.0 M MeOH at a scan rate of 100 mV/s between -1.0 V - 2.0 V at room temperature. Figure 4.11 and Figure 4.12 show cyclic voltammograms of N-doped Fe/rGO and N-doped FeNi/rGO catalysts respectively.

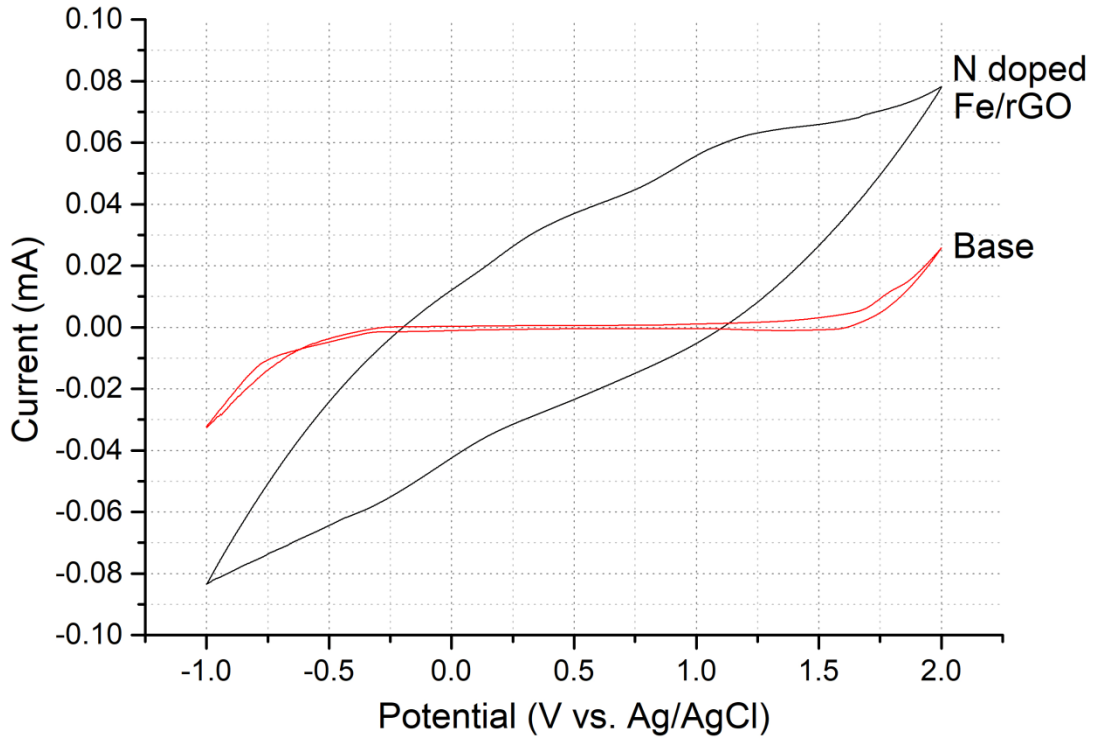

Figure 4.11 Cyclic voltammogram of N-doped Fe/rGO

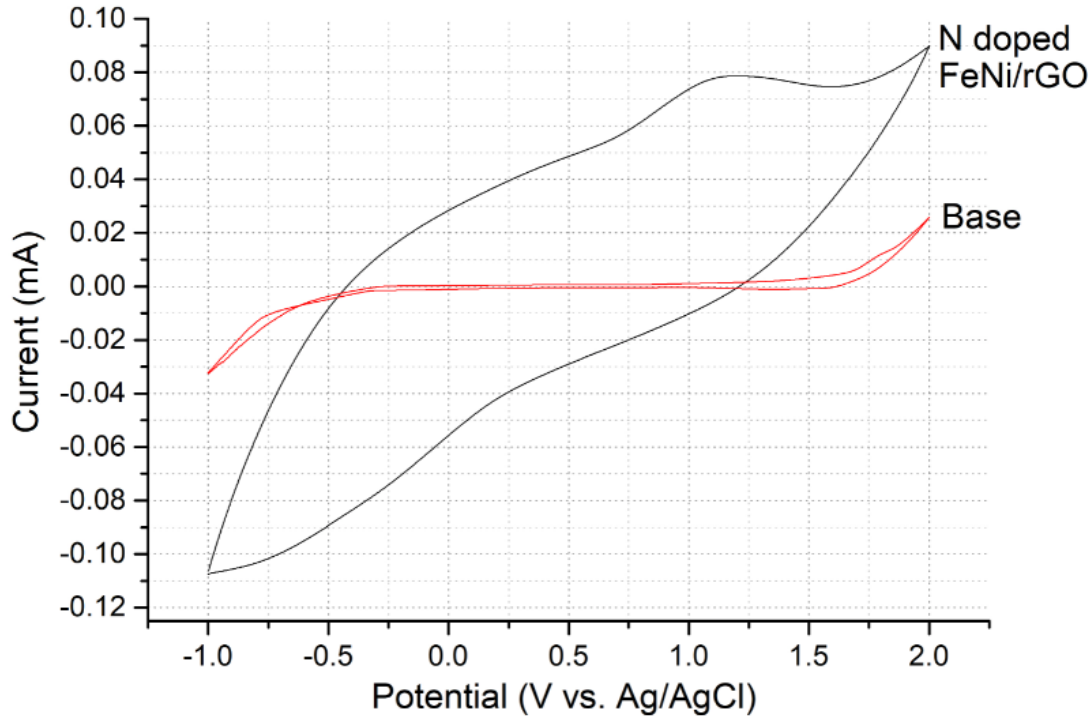

Figure 4.12 Cyclic voltammogram of N-doped FeNi/rGO

In the cyclic voltammogram of the N-doped Fe/rGO, two forward oxidation peak currents at around 0.4 V and 1.2 V during the forward scan and one backward oxidation peak current at around 0.2 V during the backward scan were observed. In the cyclic voltammogram of the N-doped FeNi/rGO, one forward oxidation peak current at around 1.1 V during the forward scan and one backward oxidation peak current at around 0.3 V during the backward scan were observed.

The one forward oxidation peak current in the cyclic voltammogram of the N-doped FeNi/rGO catalyst, occurring at around 1.1 V during the forward scan, can be evaluated as the direct electro-oxidation of methanol to CO_2 without CO formation. The two forward oxidation peak currents in the cyclic voltammogram of the N-doped Fe/rGO catalyst, occurring at around 0.4 V and 1.2 V during the forward scan, can be interpreted as the formation of CO in the first stage as a result of the electro-oxidation of methanol and the oxidation of the CO to CO_2 in the second stage. Furthermore, the forward oxidation peak occurring at around 1.1 V in the cyclic voltammogram of the N-doped FeNi/rGO catalyst has more negative voltage and

higher oxidation peak current than the forward oxidation peak occurring at around 1.2 V in the cyclic voltammogram of the N-doped Fe/rGO catalyst.

These differences may be attributed to the synergetic effect between Fe and Ni as a consequence of the modification of original active sites created by alloying (Lamy et al., 2002; Serov et al., 2013; Serov, Robson, Smolnik, et al., 2012).

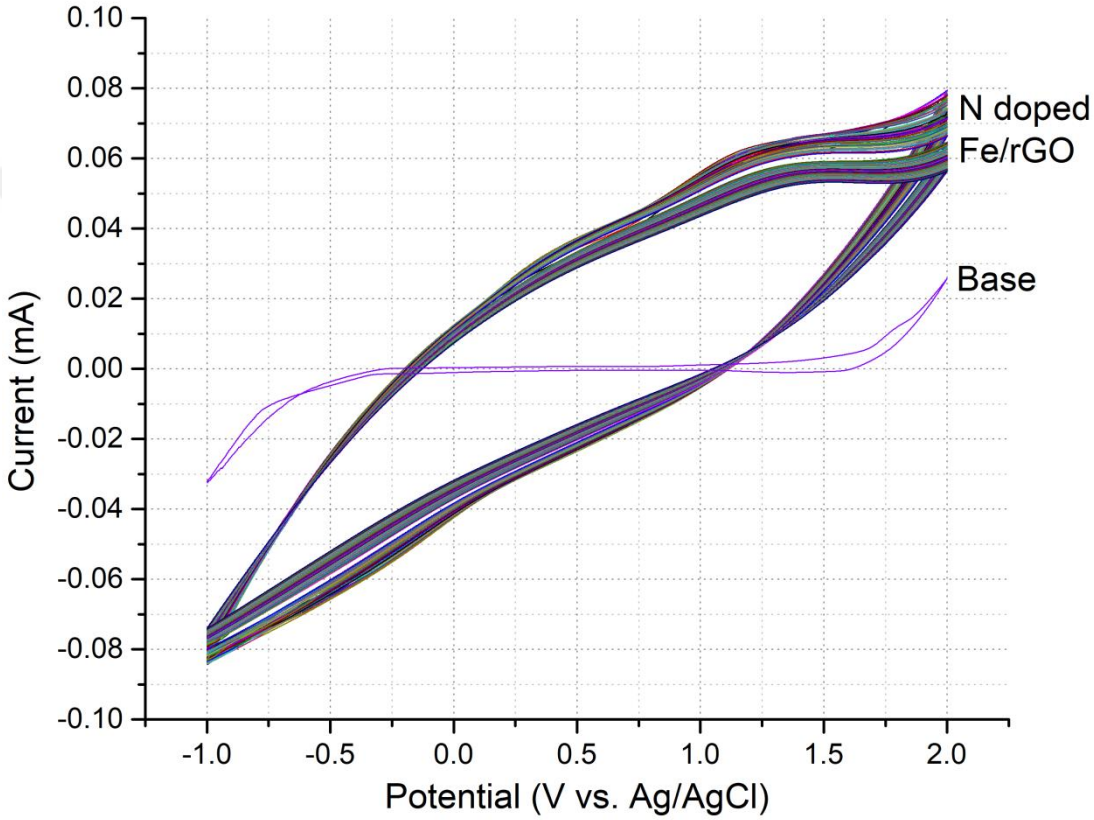

Figure 4.13 Cyclic voltammograms of N-doped Fe/rGO

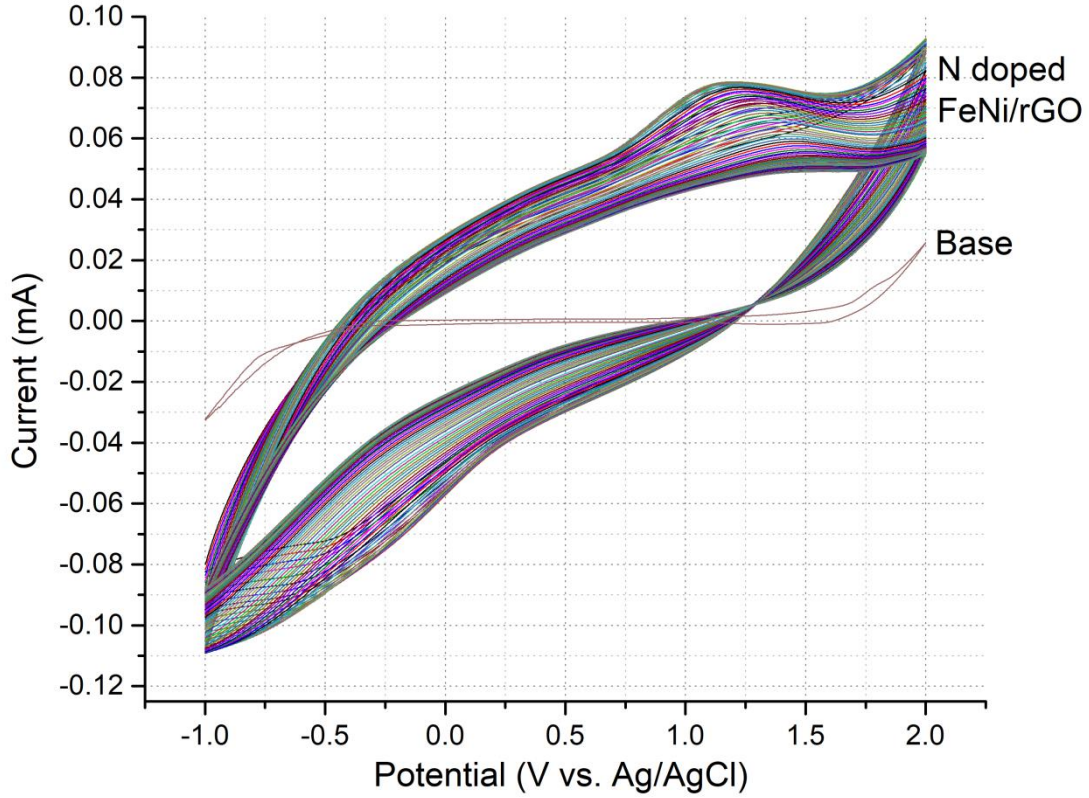

Figure 4.14 Cyclic voltammograms of N-doped FeNi/rGO

Figure 4.13 and Figure 4.14 show cyclic voltammograms of N-doped Fe/rGO and N-doped FeNi/rGO catalysts containing 100 cycles, respectively. The cyclic voltammograms of the N-doped FeNi/rGO have more fluctuation than the cyclic voltammograms of the N-doped Fe/rGO and become stable later. The high NiO amount of the N-doped FeNi/rGO catalyst probably causes this fluctuation and late stabilization. Although the N-doped FeNi/rGO catalyst has higher electrocatalytic activity than the N-doped Fe/rGO catalyst considering the obtained forward oxidation peak current, the rapid stabilization and much less fluctuation of the N-doped Fe/rGO catalyst in the cyclic voltammograms make the N-doped Fe/rGO catalyst more successful in the long term. However, when the N-doped FeNi/rGO catalyst contains a low NiO amount, it can be superior to the N-doped Fe/rGO catalyst in terms of electrocatalytic activity in the long term.

The graphene support surrounding the metal nanoparticles has a direct role in the durability and stability of the catalysts during the electrochemical measurements in

the acidic environment (Kabir et al., 2016; Tylus et al., 2014). Besides, the non-PGM catalysts made by the SSM presented almost constant performance regardless of the high methanol concentration in alkaline and acidic media contrary to the sudden performance variation of Pt/C catalyst (Sebastián et al., 2016; Tang et al., 2016).

In different electrocatalytic experiments, cyclic voltammograms having forward oxidation peak between 0.3 V – 0.8 V were obtained by using various Pt electrocatalysts in 0.5 M H_2SO_4 electrolyte containing 1 M MeOH (Cui, Li, & Liu, 2018; Guo, Zheng, Liu, Friedrich, & Garche, 2006; Li, Gao, Ci, Wang, & Ajayan, 2010; Long, Hien, Asaka, Ohtaki, & Nogami, 2011; Long, Ohtaki, Hien, Randy, & Nogami, 2011; Sim, Lim, Kwen, & Choi, 2011; Wei et al., 2017; Yang, Sim, Kwen, & Choi, 2011). However, differences among the electrocatalytic experiments, such as scan rate which is one of the parameters affecting the final current, and components used in the preparation of catalyst electrodes and their ratios make it impossible to benchmark cyclic voltammograms one-to-one.

$$i_p = 0.446nFAC^0\left(\sqrt[2]{\frac{nFvD_0}{RT}}\right) \tag{4.2}$$

As given in Equation (4.2), the Randles-Sevcik equation shows that the peak current i_p grows in direct proportion to the square root of the scan rate v (Vs^{-1}) for the electrochemically reversible electron transfer process which comprising freely diffusing redox species. Other parameters in the Equation (3.2) are the number of electrons transferred in the redox event n, the electrode surface area A (cm^2), the diffusion coefficient of the oxidized analyte D_0 ($cm^2.s^{-1}$), and the bulk concentration of the analyte C^0 ($mol.cm^{-3}$). Also, F is Faraday's constant, R is the universal gas constant, and T is the temperature (Elgrishi et al., 2018).

Nafion is used not only as a polymer electrolyte membrane in fuel cells but also as a component in certain proportions in the preparation of catalyst electrodes. It was found that 1 $mg.cm^{-2}$ Nafion loading significantly increased the electrocatalytic activity, but more than 1 $mg.cm^{-2}$ Nafion loading caused a decrease in the

electrocatalytic activity by blocking the reactant transportation (Lai, Lin, Ting, Chyou, & Hsueh, 2008).

Furthermore, the catalytic efficiency should not be evaluated only with respect to the oxidation peak currents obtained. Oxidation peak currents should be obtained at as low voltages as possible (Corti & Gonzales, 2014). The ability to obtain oxidation peak currents at low voltages indicates that electron transfer kinetics can be easily performed between the analyte and the catalyst electrode (Elgrishi et al., 2018).

CHAPTER FIVE
CONCLUSIONS

Non-precious N-doped FeNi/rGO and N-doped Fe/rGO catalysts are produced via a combination of sacrificial support method and wet impregnation method as alternative anode catalysts to precious metal catalysts of the DMFCs for electro-oxidation of methanol in acidic media.

The Marcano method used for the production of GO is found to be very efficient and practical due to the obtained interlayer distance of GO layers (7.92 Å) without extra exfoliation process.

Nitrogen doping is accomplished by the pyrolysis of urea, which also provides the reduction of graphene oxide support simultaneously. The fact that both catalysts are mainly composed of pyridinic nitrogen and Fe-Nx species proves that urea, which is the preferred organic precursor, is very successful in the nitrogen doping.

The N-doped FeNi/rGO and N-doped Fe/rGO catalysts are observed to have a 3D porous structure with homogeneously dispersed metal nanoparticles. The 3D porous structure of the catalysts is created by the sacrificial support method by removing the silica template.

The determined mixing ratio and heat treatment temperature for the precursors and silica used in the catalyst production are found suitable to produce catalysts having a 3D porous structure and Fe-Nx species.

The presence of the Fe-Ni alloy in the bi-metallic N-doped FeNi/rGO catalyst is determined.

The methanol electro-oxidation in acidic media is realized by the catalysts produced. The forward oxidation peak currents obtained at high voltages indicate that the catalysts produced do not have as high electrocatalytic activity as platinum.

However, it should be remembered that the catalyst electrodes prepared with the catalysts produced do not contain Nafion, a component that increases the electrocatalytic activity.

The low Fe-Ni alloy ratio and high NiO amount of the N-doped FeNi/rGO catalyst do not make the synergetic effect between Fe and Ni strikingly visible.

The catalysts with high Fe-Ni alloy ratio and electrocatalytic activity can be produced using different mixing ratios, heat treatment temperatures, and silica templates. The catalyst electrodes prepared with these catalysts and the Nafion component may have great performance in electrocatalytic experiments.

The fact that the prepared catalysts contain high amounts of pyridinic nitrogen and Fe-Nx centers and low amounts of pyrrolic nitrogen, quaternary nitrogen, and graphitic nitrogen centers indicates that they can be used also as cathode catalysts for ORR in acidic media.

REFERENCES

Alam, S. N., Sharma, N., & Kumar, L. (2017). Synthesis of graphene oxide (GO) by modified hummers method and its thermal reduction to obtain reduced graphene oxide (rGO). *Graphene*, *6*(1), 1–18.

Atanassov, P. (2014, April). Keynote Presentation: Fuel Cells Electrocatalysts Derived By Sacrificial Support Method (SSM). In *Meeting Abstracts* (No. 4, pp. 516-516). The Electrochemical Society.

Barakat, N. A. M., El-Deen, A. G., Ghouri, Z. K., & Al-Meer, S. (2018). Stable N-doped & FeNi-decorated graphene non-precious electrocatalyst for oxygen reduction reaction in acid medium. *Scientific Reports*, *8*(1), 1–11.

Chen, J., Yao, B., Li, C., & Shi, G. (2013). An improved Hummers method for eco-friendly synthesis of graphene oxide. *Carbon*, *64*(1), 225–229.

College of the Desert, & SunLine Transit Agency. (2001). Hydrogen fuel cell engines and related technologies course manual - module 4: Fuel cell technology, 1–62. Retrieved December 20, 2018, from https://www1.eere.energy.gov/hydrogenandfuelcells/tech_validation/h2_manual.html

Corti, H. R., & Gonzalez, E. R. (2014). Introduction to direct alcohol fuel cells. In *Direct Alcohol Fuel Cells* (pp. 1-32). Springer, Dordrecht.

Cote, L. J., Cruz-Silva, R., & Huang, J. (2009). Flash reduction and patterning of graphite oxide and its polymer composite. *Journal of the American Chemical Society*, *131*(17), 11027–11032.

Cui, H., Li, Y., & Liu, S. (2018). N, P-codoped mesoporous carbon supported PtCox nanoparticles and their superior electrochemical toward methanol oxidation. *IOP*

Conference Series: Earth and Environmental Science, *128*(1).

Dimiev, A. M., Alemany, L. B., & Tour, J. M. (2013). Graphene oxide. Origin of acidity, its instability in water, and a new dynamic structural model. *American Chemical Society Nano*, *7*(1), 576–588.

El-Deen, A. G., El-Newehy, M., Kim, C. S., & Barakat, N. A. M. (2015). Nitrogen-doped, FeNi alloy nanoparticle-decorated graphene as an efficient and stable electrode for electrochemical supercapacitors in acid medium. *Nanoscale Research Letters*, *10*(1), 1–7.

Elgrishi, N., Rountree, K. J., McCarthy, B: D., Rountree, E. S., Eisenhart, T. T., & Dempsey, J. L. (2018). A practical beginner's guide to cyclic voltammetry. *Journal of Chemical Education*, *95*(2), 197-206.

Emiru, T. F., & Ayele, D. W. (2017). Controlled synthesis, characterization and reduction of graphene oxide: A convenient method for large scale production. *Egyptian Journal of Basic and Applied Sciences*, *4*(1), 74-79.

Guo, Y., Zheng, D., Liu, H., Friedrich, A., & Garche, J. (2006). Investigation of bifunctional mechaniscm in methanol oxidation on carbon-support Pt and Pt-Ru catalysts. *Journal of New Materials for Electrochemical Systems*, *9*(1), 33-39.

Jing, P., Liu, M., Pu, Y., Cui, Y., Wang, Z., Wang, J., & Liu, Q. (2016). Dependence of phase configurations, microstructures and magnetic properties of iron-nickel (Fe-Ni) alloy nanoribbons on deoxidization temperature in hydrogen. *Scientific Reports*, *6*, 37701.

Kabir, S., Serov, A., Artyushkova, K., & Atanassov, P. (2016). Design of novel graphene materials as a support for palladium nanoparticles: Highly active catalysts towards ethanol electrooxidation. *Electrochimica Acta*, *203*, 144–153.

Kim, S. K., Park, J. Y., Hwang, S. C., Lee, D. K., Lee, S. H., Han, M. H., & Rhee, Y. W. (2014). Radiolytic preparation of electrocatalysts with Pt-Co and Pt-Sn nanoparticles for a proton exchange membrane fuel cell. *Journal of Nanomaterials, 2014*, 15.

Lai, C. M., Lin. J. C., Thing, F. P., Chyou, S. D., & Hsueh, K. L. (2008). Contribution of Nafion loading to the activity of catalysts and the performance of PEMFC. *International Journal of Hydrogen Energy*, *33*(15), 4132-4137.

Lamy, C., Lima, A., LeRhun V., Delime, F., Coutanceau, C., & Léger, J.-M. (2002). Recent advances in the development of direct alcohol fuel cells (DAFC). *Journal of Power Sources*, *105*(2), 283–296.

Li, D., Duan, X., Sun, H., Kang, J., Zhang, H., Tade, M. O., & Wang, S. (2017). Facile synthesis of nitrogen-doped graphene via low-temperature pyrolysis: The effects of precursors and annealing ambience on metal-free catalytic oxidation. *Carbon*, *115*(January), 649–658.

Li, J., Zeng, X., Ren, T., & van der Heide, E. (2014). The preparation of graphene oxide and ıts derivatives and their application in bio-tribological systems. *Lubricants*, *2*(3), 137–161.

Li, J., Zhang, D., Qi, H., Wang, G., Tang, J., Tian, G., & Feng, S. (2018). Economical synthesis of composites of FeNi alloy nanoparticles evenly dispersed in two-dimensional reduced graphene oxide as thin and effective electromagnetic wave absorbers. *Royal Society of Chemistry Advances*, *8*(15), 8393–8401.

Li, X., Wang, H., Robinson, J. T., Sanchez, H., Diankov, G., & Dai, H. (2009). Simultaneous nitrogen doping and reduction of graphene oxide. *Journal of American Chemical Society*, *131*(43), 15939–15944.

Li, Y., Gao, W., Ci, L., Wang, C., & Ayajan, P. M. (2010). Catalytic performance of

Pt nanoparticles on reduced graphene oxide for methanol electro-oxidation. *Carbon*, *48*(4), 1124-1130.

Liu, Y., Zhao, Y. L., Gao, Z. F., Jiang, X., & Zeng, Y. P. (2013). Facile synthesis and supercapacitor properties of graphene nanosheets. *Journal of Inorganic Materials*, *28*(6), 611–615.

Long, N. V., Hien, T. D., Asaka, T., Ohtaki, M., & Nogami, M. (2011). Synthesis and characterization of Pt-Pd alloy and core-shell bimetallic nanoparticles for direct methanol fuel cells (DMFCs): Enhanced electrocatalytic properties of well-shaped core-shell morphologies and nanostructures. *International Journal of Hydrogen Energy*, *36*(14), 8478-8491.

Long, N. V., Ohtaki, M., Hien, T. D., Randy, J., & Nogami, M. (2011). A comparative study of Pt and Pt-Pd core-shell nanocatalysts. *Electrochemica Acta*, *56*(25), 9133-9143.

Long, N. V., Thi, C. M., Nogami, M., & Ohtaki, M. (2012). Novel Pt and Pd based core-shell catalysts, with critical new issues of heat treatment, stability and durability for proton exchange membrane fuel cells and direct methanol fuel cells. In F. Czerwinski, (Ed.). *Heat treatment – conventional and novel applications* (41-74). Rijeka: InTech.

Marcano, D. C., Kosynkin, D. V., Berlin, J. M., Sinitskii, A., Sun, Z., Slesarev, A., & Tour, J. M. (2010). Improved synthesis of graphene oxide. *American Chemical Society Nano*, *4*(8), 4806–4814.

Monshi, A., Foroughi, M. R., & Monshi, M. R. (2012). Modified Scherrer equation to estimate more accurately nano-crystallite size using XRD. *World journal of nano science and engineering*, *2*(3), 154-160.

Pei, S., & Cheng, H. M. (2012). The reduction of graphene oxide. *Carbon*, *50*(9),

3210–3228.

Pendolino, F., & Armata, N. (2017). Characterization and models of graphene oxide. In *Graphene oxide in environmental remediation process*. Synthesis (5-21). Cham: Springer Nature.

Robson, M. H., Serov, A., Artyushkova, K., & Atanassov, P. (2013). A mechanistic study of 4-aminoantipyrine and iron derived non-platinum group metal catalyst on the oxygen reduction reaction. *Electrochimica Acta*, *90*, 656–665.

Sebastián, D., Serov, A., Artyushkova, K., Atanassov, P., Aricò, A. S., & Baglio, V. (2016). Performance, methanol tolerance and stability of Fe-aminobenzimidazole derived catalyst for direct methanol fuel cells. *Journal of Power Sources*, *319*, 235–246.

Sebastián, D., Serov, A., Matanovic, I., Artyushkova, K., Atanassov, P., Aricò, A. S., & Baglio, V. (2017). Insights on the extraordinary tolerance to alcohols of Fe-N-C cathode catalysts in highly performing direct alcohol fuel cells. *Nano Energy*, *34*(December 2016), 195–204.

Serov, A., Andersen, N. I., Kabir, S. A., Roy, A., Asset, T., Chatenet, M., Maillard, F., & Atanassov, P. (2015). Palladium supported on 3D graphene as an active catalyst for alcohols electrooxidation. *Journal of The Electrochemical Society*, *162*(12), F1305-F1309.

Serov, A., Artyushkova, K., Andersen, N. I., Stariha, S., & Atanassov, P. (2015). Original mechanochemical synthesis of non-platinum group metals oxygen reduction reaction catalysts assisted by sacrificial support method. *Electrochimica Acta*, *179*, 154–160.

Serov, A., Artyushkova, K., & Atanassov, P. (2014). Fe-N-C oxygen reduction fuel cell catalyst derived from carbendazim: Synthesis, structure, and reactivity.

Advanced Energy Materials, *4*(10), 1–7.

Serov, A., Robson, M. H., Artyushkova, K., & Atanassov, P. (2012). Templated non-PGM cathode catalysts derived from iron and poly(ethyleneimine) precursors. *Applied Catalysis B: Environmental*, *127*, 300–306.

Serov, A., Robson, M. H., Halevi, B., Artyushkova, K., & Atanassov, P. (2012). Highly active and durable templated non-PGM cathode catalysts derived from iron and aminoantipyrine. *Electrochemistry Communications*, *22*(1), 53–56.

Serov, A., Robson, M. H., Smolnik, M., & Atanassov, P. (2012). Templated bi-metallic non-PGM catalysts for oxygen reduction. *Electrochimica Acta*, *80*, 213–218.

Serov, A., Robson, M. H., Smolnik, M., & Atanassov, P. (2013). Tri-metallic transition metal-nitrogen-carbon catalysts derived bysacrificial support method synthesis. *Electrochimica Acta*, *109*, 433–439.

Sim, K. S., Lim, S. M., Kwen, H. D., & Choi, S.H. (2011). Electrocatalytic activity for CO, MeOH, and EtOH oxidation on the surface Pt-Ru nanoparticles supported by metal oxide. *Journal of Nanomaterials*, *2011*(614983).

Stariha, S., Artyushkova, K., Workman, M. J., Serov, A., Mckinney, S., Halevi, B., & Atanassov, P. (2016). PGM-free Fe-N-C catalysts for oxygen reduction reaction: Catalyst layer design. *Journal of Power Sources*, *326*, 43–49.

Tang, S., Zhou, X., Xu, N., Bai, Z., Qiao, J., & Zhang, J. (2016). Template-free synthesis of three-dimensional nanoporous N-doped graphene for high performance fuel cell oxygen reduction reaction in alkaline media. *Applied Energy*, *175*, 405–413.

Technical University of Denmark. (2019). *Polymer electrolyte membrane fuel cells*.

Retrieved February 15, 2019, from http://www.ele.energy.dtu.dk/Research/Fuel-cells.

Tylus, U., Jia, Q., Strickland, K., Ramaswamy, N., Serov, A., Atanassov, P., & Mukerjee, S. (2014). Elucidating oxygen reduction active sites in pyrolyzed metal-nitrogen coordinated non-precious-metal electrocatalyst systems. *Journal of Physical Chemistry C*, *118*(17), 8999–9008.

Wei, D., Liu, Y., Wang, Y., Zhang, H., Huang, L., & Yu, G. (2009). Synthesis of N-doped graphene by chemical vapor deposition and ıts electrical properties. *Nano Letters*, *9*(5), 1752-1758.

Wei, Q., Zhang, G., Yang, X., Chenitz, R., Banham, D. W. H., Yang, Li., et al. (2017). 3D porous Fe/Ni/C spherical nanostructures as high-performance electrocatalysts for oxygen reduction in both alkaline and acidic media. *American Chemical Society Applied Materials & Interfaces*, *9*(42), 36944-36954.

Xu, Y., Li, J., & Huang, W. (2017). Porous graphene oxide prepared on nickel foam by electrophoretic deposition and thermal reduction as high-performance supercapacitor electrodes. *Materials*, *10*(8).

Yang, D. S., Sim, K. S., Kwen, H. D., & Choi, S.H. (2011). Radiolytic synthesis of Pt-Ru catalysts based on functional polymer-grafted MWNT and their catalytic efficiency for CO and MeOH. *Journal of Nanometarials, 2011*(134721).

Yang, L., Zeng, X., Wang, D., & Cao, D. (2018). Biomass-derived FeNi alloy and nitrogen-codoped porous carbons as highly efficient oxygen reduction and evolution bifunctional electrocatalysts for rechargeable Zn-air battery. *Energy Storage Materials*, *12*, 277–283.

Zaaba, N. I., Foo, K. L., Hashim, U., Tan, S. J., Liu, W. W., & Voon, C. H. (2017). Synthesis of Graphene Oxide using Modified Hummers Method: Solvent

Influence. *Procedia Engineering*, *184*, 469–477.